Journal of the European Ceramic Society 46 (2026) 117741

Contents lists available at ScienceDirect

Journal of the European Ceramic Society

journal homepage: www.elsevier.com/locate/jeurceramsoc

Review article

Sinter-based perovskites for energy-related applications

Carina Hedrich [a], Stefane V. Besegatto [a], Sergio Y.G. González [b], Kaline P. Furlan [a,c,*]

[a] Hamburg University of Technology, Integrated Ceramic-based Materials Systems Group, Denickestrasse 15, Hamburg 21073, Germany
[b] Federal University of Santa Catarina (UFSC), Chemical and Food Engineering Department, Trindade Campus, Florianópolis, SC 88040-900, Brazil
[c] Karlsruhe Institute of Technology (KIT), Institute for Applied Materials – Ceramic Materials and Technologies, Karlsruhe 76131, Germany

ARTICLE INFO

Keywords:
Perovskites
Sintering
Energy storage
Energy conversion
Energy generation

ABSTRACT

The transition to a low-carbon economy stands as one of the most pressing global challenges today. Developing innovative, more efficient, and sustainable material systems for energy generation, conversion, or storage are key-enabling technologies to solve this challenge. Perovskites, with their unique structural and functional properties, emerge as next-generation materials capable of addressing various energy-related applications. This review focuses on recent progress in their synthesis via sintering and emphasizes how processing parameters modify their microstructure and consequently, can enhance their performance in diverse energy storage technologies, including capacitors, supercapacitors, batteries, and energy conversion systems. Moreover, by identifying current challenges of sinter-based perovskites and outlining future directions this review offers a comprehensive overview of the latest advancements and potential of sinter-based perovskites in the field of energy materials research.

1. Introduction

Perovskite is a general term used to denote a class of complex compounds characterized by the standard molecular formula ABX_3 and where the elements share the same crystallographic structure [1]. This family's materials can be categorized into two main subsets: inorganic oxide perovskites and halide perovskites. The perovskite structural flexibility allows for substantial cationic substitutions within their network, which give rise and access to unique properties. This structural versatility enables various applications [2] ranging from piezoelectric elements [3], sensors [4], and capacitors [5,6] to solid oxide fuel cells for energy generation [7,8].

The synthesis of perovskite materials is decisive for their intended application because the perovskites' (micro-)structure and morphology dictate their functional properties [9–18]. Various synthesis methods have been reported for perovskites including the classical route of powder fabrication followed by sintering [14,18]. Moreover, recent developments apply thin film deposition techniques such as pulsed laser deposition, chemical vapor deposition, atomic layer deposition, and solution-based spin coating for fabricating perovskite films [12,14,18,19]. Additionally, combustion synthesis and spray and freeze drying gain increasing interest for fabricating complex perovskite structures [18,19]. Despite the recent developments of applying new synthesis methods, the classical fabrication route is widely used for perovskites for energy-related applications [12,14]. Furthermore, precise optimization and fine-tuning of the two involved steps – powder fabrication and sintering – can significantly enhance the functional properties of perovskites synthesized via this route.

The perovskites' microstructure is largely influenced by the sintering process. Sintering in general denotes a thermal treatment applied to densify powders by diffusion-controlled mechanisms below the materials' melting point [20]. Sintering conditions, namely sintering method, temperature, heating rate, dwell time, and atmosphere, are crucial parameters for controlling grain growth, phase composition, and porosity evolution of the perovskites [21]. These morphological and microstructural characteristics determine the functional properties of perovskites, e.g., conductivity, mechanical strength, and chemical stability, and consequently their performance in energy-related applications [14,16]. Progress in sintering methods have expanded the possibilities to tailor perovskites for increasing their performance. While conventional solid-state sintering is still widely employed, it often requires prolonged treatments at elevated temperature which can result in undesired structural changes such as grain growth and secondary phase formation [20,22–24]. Emerging sintering techniques such as liquid phase sintering and spark plasma sintering enable material densification at lower temperatures and shorter times [20,25–29]. Hence, nanoscale features

* Corresponding author at: Hamburg University of Technology, Integrated Ceramic-based Materials Systems Group, Denickestrasse 15, Hamburg 21073, Germany.
E-mail address: kaline.furlan@kit.edu (K.P. Furlan).

https://doi.org/10.1016/j.jeurceramsoc.2025.117741
Received 25 March 2025; Received in revised form 30 July 2025; Accepted 8 August 2025
Available online 9 August 2025

of perovskite materials are often preserved whereby the mechanical properties and electronic/ionic conductivity are enhanced. A detailed understanding of structure-function relationships in sinter-based perovskites is crucial to improve their performance in energy-related applications, for instance batteries, capacitors, supercapacitors, solid oxide fuel cells, and solid oxide electrolyte cells.

This review provides an overview of sinter-based perovskites as functional materials in energy-related applications as schematically outlined in Fig. 1. Section 2 summarizes the general structure of perovskites and explains the special features of layered perovskites and halide perovskites. Since sinter-based perovskites are prepared by a two-step process involving powder fabrication followed by sintering, synthesis methods for perovskite powders are explained in Section 3. In Section 4, the key characteristics of three different sintering methods – conventional solid-state sintering, liquid phase sintering, and spark plasma sintering, are briefly summarized and examples of perovskite fabrication with these methods are given. Section 5 focuses on sinter-based perovskites applied in energy storage applications, namely batteries, capacitors, and supercapacitors. Applications of sinter-based perovskites in energy conversion and generation as solid oxide fuel cells and solid oxide electrolyte cells are presented in Section 6. Finally, Section 7 summarizes the reviewed studies and outlines future perspectives of sinter-based perovskites in energy-related applications.

2. Structure of perovskites

An ideal perovskite, as the one with the structure of $CaTiO_3$, exhibits cubic symmetry, as illustrated in Fig. 2, where larger ions are accommodated in the A-site and smaller ions in the B-site. Generally, the A-site contains ions with an A^{2+} charge, such as rare earths, alkali metals, alkaline earth metals, and other ions with larger particle radius [10]. Meanwhile, the B-site typically contains ions with a B^{4+} charge, mainly composed of transition metal from the third, fourth, and fifth periods, and the X is composed by an oxygen group or halogen [30]. In the ABO_3 crystal, the A-site is coordinated with twelve oxygen atoms and occupies the central position within the cube, whilst the B-site adopts a coordination arrangement involving six oxygen atoms in an octahedral configuration $[BO_6]$ [1,31].

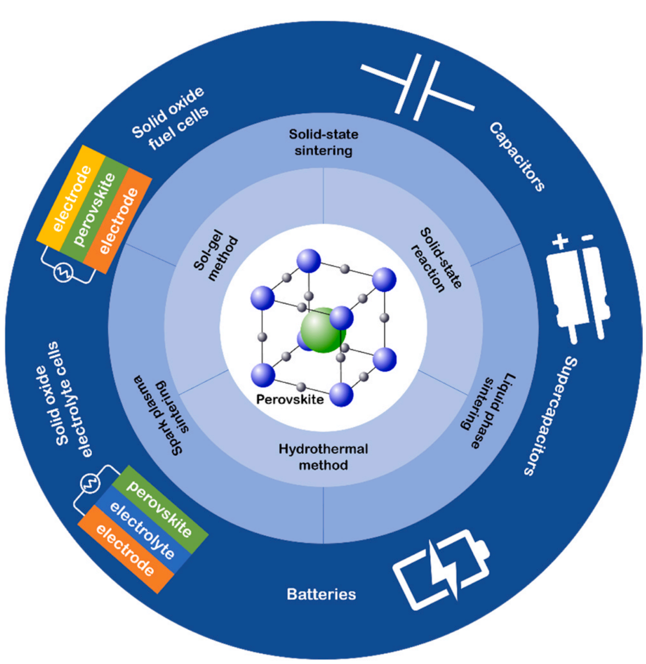

Fig. 1. This review focuses on sinter-based perovskites for energy-related applications from their synthesis (inner and middle ring) towards the application (outer ring). The influence of sintering parameters on the functional properties is highlighted in this article.

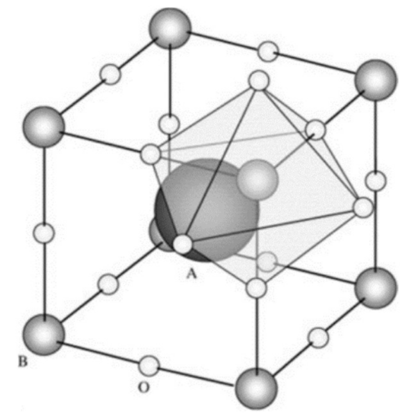

Fig. 2. Schematic of an ABO_3 perovskite cell. Figure adapted with permission [9]. Copyright 2001, Elsevier.

Nonetheless, the ABO_3 configuration depends on two main criteria: electroneutrality and ionic radii size. To achieve electroneutrality in ABO_3, ions A and B can be categorized into five distinct groups based on the charges at sites A and B represented by the following pairs of ions: (+1, +5), (+2, +4), (+3, +3), (+4, +2), and (+5, +1). In theory, there are 2346 potential combinations for ABO_3, but only about 265 have been reported experimentally in the literature [10,32].

Given the extensive range of metallic elements capable of successfully incorporating into A and B sites with diverse oxidation states, the vast chemical space results in several possible compositions. The geometric configuration of an ideal cubic perovskite can be lowered to an alternative crystal arrangement (e.g., orthogonal, tetragonal, etc.) due to rotation and tilting of the $[BO_6]$ octahedra [33]. To maintain the geometrical configuration of an ideal perovskite structure, A and/or B substitution candidates should possess similar ionic radius within Goldschmidt's tolerance factor (t), calculated according to the formula shown in Eq. 1, where R_A, R_B, and R_X are the ionic radii of A, B and X, respectively.

$$t = \frac{R_A + R_B}{\sqrt{2}(R_B + R_X)} \tag{1}$$

Normally, at ambient temperature, the structure remains cubic if t is in between 0.85 and 1. If the ionic radius of element A is smaller than its ideal value, t decreases below 1 resulting in orthorhombic, tetragonal, or rhombohedral deformations [33,34]. However, when the t exceeds 1 due to a large or a small atom at an A and B sites, respectively, a tetragonal structure is typically observed. These lattice distortions and alterations are common among perovskites [35], influencing their physicochemical properties such as dielectric, electrical, magnetic, and optoelectronic properties, thus influencing these materials' applications [34]. Therefore, the investigations regarding their crystal structures and resulting properties constitute a research field in constant evolution within materials science.

In addition, the structural and compositional flexibility of perovskites can also induce the appearance of spontaneous polarization of other types of crystal structures [36]. However, substantial deviation from this ideal ratio can be tolerated at the expense of geometrical distortions, the interatomic lengths (A-X and B-X) in the cubic perovskite structure are congruent $\left(\sqrt{2d_{B-X}} = d_{A-X}\right)$ [37]. In some instances, when the distortion reaches a critical level, some of the three-dimensional B-X bonds can break [32] and consequently disrupt the network, forming new bonds that are one-dimensional (1D) or two-dimensional (2D) rather than the original 3D configuration [38]. This phenomenon gives rise to perovskite derivatives with altered structural dimensionalities, such as layered perovskite materials (Ruddlesden-Popper, Aurivillius, Dion–Jacobson) [31,39] and oxygen-deficient brownmillerite compounds [30,40].

2.1. Layered perovskites

Layered perovskite materials are derived from the ideal cubic perovskite oxides, having 2D layers of ABO_3 configuration forming a structure composed of corner-sharing BO_6 octahedra and 12-coordinated A cations located at the interstitial lattice sites [38]. In essence, the compositional model of layered perovskite materials can be elucidated through several general formulas, each defining a unique phase of these structures, where n represents the number of BO_6 octahedra spanning a layer. Aurivillius phase can be described as $(Bi_2O_2)(A_{n-1}B_nO_{3n+1})$, Ruddlesden-Popper phase as $A_{n+1}B_nO_{3n+1}$ or $A'_2A_{n-1}B_nO_{3n+1}$, and Dion–Jacobson phase as $A'(A_{n-1}BnO_{3n+1})$ [1,40].

The flexible layered configuration facilitates the development of hybrid systems, creating a broad spectrum of new potential applications. Moreover, some layered perovskites exhibit remarkable stability and possess conduction bands significantly above the H^+ reduction potential, thus holding promise for hydrogen (H_2) generation [38]. For Aurivillius phases, their structure contains n (1 to 5) perovskite octahedral layers $(A_{n-1}B_nO_{3n+1})_{2-}$ sandwiched between sheets of bismuth-oxygen $(Bi_2O_2)^{2+}$ [31]. Ruddlesden-Popper (RP) $A_2A_{n-1}BnO_{3n+1}$ is characterized by a repeating sequence of perovskite and rock-salt-like (A'O) layers. The layered structure combined with the versatility in chemical composition due to the variable 'A' and 'B' cations can lead to interesting properties such as magnetoresistance, superconductivity, ferroelectricity, and catalytic activity [41]. For example, $La_{0.6}Sr_{1.4}MnO_4$ [42] and Li_2NiO_4 [43] exhibit mixed ionic and electronic conductivity, appropriate electrochemical activity, and suitable chemical and mechanical compatibilities with solid oxide fuel cell components [44,45].

2.2. Metal halide perovskites

Halide perovskites, a subject of research spanning over six decades since Møller's pioneering work in 1958 [46], have gained significant attention in recent years due to their interesting properties, such as considerable absorption coefficient, long diffusion length, small exciton binding energy, and tunable energy band-gap [47]. These attributes enable their potential use in energy conversion technologies, including solar cells, supercapacitors, light-emitting diodes, photodetectors, and field-effect transistors [48]. Consequently, both halide perovskites forms have attracted much research attention: hybrid organic-inorganic halide perovskites (HHPs) and inorganic halide perovskites (IHPs). The chemical nature, organic or inorganic, of the ions in the A site of the perovskite indicates the difference between both [49].

Halide perovskites can also be described using the general structure ABX_3. An ideal organic–inorganic perovskite possesses a cubic cell with the general formula AMX_3, where A represents a monovalent organic or inorganic cation (e.g. Cs^+, methylammonium MA^+ or formamidinium FA^+), M represents a bivalent cation (e.g. Sn^{2+}, Pb^{2+}), and X represents halide anion (e.g. Cl^-, Br^-, I^-) [49,50]. The crystal structure $MAPbI_3$ exemplifies a configuration wherein the eight corners of the cubic structure are occupied by methylammonium ions ($MA^+ = CH_3NH^{3+}$), and the X lattice sites are filled with iodide ions (I^-), effectively maintaining charge neutrality within the PbI_6 network. This composition of lead-based hybrid perovskites ($CH_3NH_3PbI_3$) stands out in the family of organic-inorganic metal halide perovskites [51] due to its bandgap value around 1.5–1.6 eV associated with a more extended light absorption spectrum (wavelength > 800 nm). Therefore, these materials have found widespread applications in photovoltaic systems and as photocatalysts for energy generation [52]. However, $MAPbI_3$ exhibit low formation energy, making them susceptible to degradation and lacking environmental stability, particularly when exposed to heat, UV radiation, and humidity [1,39]. Moreover, they can adversely affect the environment due to the presence of elements that can contaminate the soil and water reservoirs when leached [48]. While this characteristic poses a clear disadvantage, it also paves the way for research to improve their stability.

3. Synthesis of perovskite powders

Precise control over perovskite structure and morphology is crucial to optimizing their performance in energy systems. These characteristics depend highly on the synthesis method and potential further processing steps. Various synthesis techniques have been utilized to fabricate perovskite materials, including solid-state reaction, co-precipitation, sol-gel, and hydrothermal synthesis [13]. As the review focuses on sinter-based perovskites, this section presents the most common synthesis routes for fabricating perovskite powders, which can be later shaped and sintered.

3.1. Sol-gel method

The sol-gel method involves forming an amorphous gel, followed by particle nucleation and growth, gel dehydration, and calcination at relatively high temperatures (1000 °C) [13,53]. Ethylene-diaminetetraacetic acid (EDTA) is often used as a chelating agent to prevent the partial segregation of metallic components, which can result from the varying interactions between metal cations in the solution [19,54,55].

The synthesis' basic mechanism entails the complexation of metal ions with EDTA/citric acid, followed by water evaporation and thermal decomposition of the solvent and complex, leading to the subsequent formation of the perovskite phase [13,56]. The resulting powder is typically non-porous, coarse, irregularly shaped, and exhibits a broad particle size distribution, with low specific surface areas [19,57], sometimes requiring post-processing for the comminution of agglomerates or particle size screening. Nevertheless, this method has been widely adopted due to its advantages, such as relatively chemically homogeneous compounds, compared to reaction-based methods [55, 57].

3.2. Solid-state reaction method

The solid-state reaction is widely used for the synthesis of perovskite materials. It involves directly mixing solid starting materials (powders) and then subjecting the mix to a calcination process to diffuse elements and promote solid-state reactions towards the final perovskite composition [18]. Such calcination is sometimes performed after shaping the powders, which is then directly followed by sintering, i.e., the solid-state reaction step is combined within the sintering process. This is generally considered a facile method, as it does not require complex equipment or chemical labs. Nevertheless, the chemical homogeneity of the final product depends on strict control of the process parameters, such as temperature, dwell time, and atmosphere. If those are not adequately controlled, it can negatively affect the perovskite properties and, thus, their final application [12]. Iriani et al. [36] recently reported synthesizing $Ba_{0.95}Sr_{0.05}TiO_3$ ceramic capacitors in solid state and co-precipitation routes with different sintering temperatures. While the solid-state route guarantees pure phase formation at 1000 °C, the co-precipitation method requires temperatures above 1200 °C. However, the analysis of structural and electrical properties of the material synthesized by the solid-state process demonstrated that less dense ceramics with larger grains were obtained when using lower sintering temperatures, leading to poorer dielectric properties with larger hysteresis. In other words, seemingly simple parameters such as dwell time and temperature can directly affect properties such as pore size distribution and surface area, which are essential for high-energy-density applications.

3.3. Hydrothermal method

In the hydrothermal method, a solution-based reaction approach is employed, wherein precursors are heated within an autoclave at elevated temperatures and pressures in the presence of H_2O as solvent [19,58]. Typically, the temperature utilized in the hydrothermal process is chosen based on the water's boiling point and the solution's critical temperature, often ranging from above 60 °C to about 400 °C [19,59,60]. The high temperature applied to the sealed vessel results in high pressure within the vessel, enhancing the reactants' solubility [60]. This technique allows reasonable control over the particle size distribution and is considered easy operation, keeping in mind that the temperature is the sole parameter to be regulated. At the same time, pressure is directly dependent on it and thus only measured [61–63].

Whereas the synthesis of "simple" perovskites is somewhat established, the synthesis of complex or high entropy multioxides is still in its infancy. For example, high-quality $CaTiO_3$ can be prepared by the hydrothermal method at 150 °C, followed by calcination at 1300 °C, presenting a homogeneous perovskite phase and no impurities [64]. Meanwhile, the research on hydrothermal synthesis at 240°C for 48 h of complex perovskites such as $La_xCa_{(1-x)}MnO_3$ and $La_xSr_{(1-x)}MnO_3$ shows that the final powder presented unreacted $La(OH)_3$ probed by X-ray diffraction (XRD). An increase in the calcination temperature from 900 °C to 1100 °C generated a perovskite-type phase but still contained impurities [61]. In another work, the perovskite electrode $Nd_{0.7}Co_{0.3}FeO_3$ achieved a pure crystalline compound at 900 °C. However, even with an increase in the calcination temperature to 1100 °C, 2.7 % of impurities associated with Co_2O_3 were detected [65]. Similar behavior

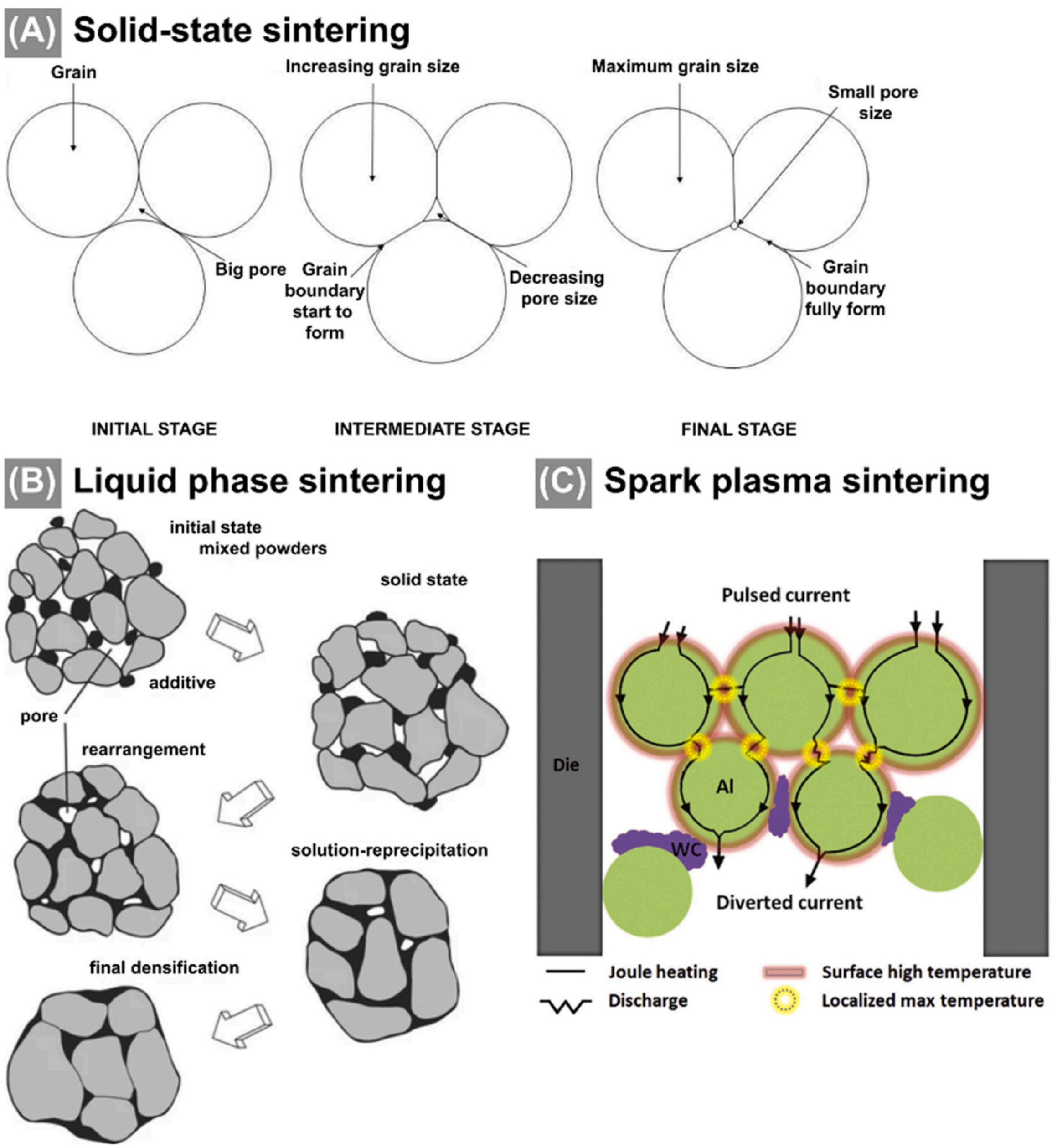

Fig. 3. Overview of different sintering mechanisms. (A) Solid-state sintering involves grain boundary formation and increasing grain sizes. These processes are associated with particle necking and reduction of pore sizes. Adapted with permission [70]. Copyright 2023, Elsevier. (B) Liquid phase sintering of powders results in grain growth and densification of the initial powder. Adapted with permission [26]. Copyright 2009, Springer. (C) Spark plasma sintering utilizes a pulsed power source to apply resistive heating to the component of interest resulting in while simultaneously applying a uniaxial mechanical load. Adapted with permission [72]. Copyright 2017, Elsevier.

was observed in other reports [63,65,66].

4. Sintering process routes for perovskites

After shaping the powders using different methods, which are outside the scope of this review, sintering is an established method for perovskites fabrication, consolidating the shaped powders into parts for a device or full components [67]. The sintering research field experienced a notable boost in the early 20th century, when electromagnetic fields, electrical currents, and radiation were introduced as facilitating tools [20,68]. Currently, both traditional and advanced sintering processes are used in many areas of research and industry, including energy-related applications.

Sintering is an essential step for manufacturing bulk as well as porous perovskites [21]. Besides providing mechanical strength, the sintering process can also be used to tailor the functional properties [21,25,69]. The most used methods to sinter perovskite materials are solid-state sintering (SSS), liquid phase sintering (LPS), and spark plasma sintering (SPS). Fig. 3 illustrates the primary differences among these routes. The following subsections present concise descriptions of these sintering routes and focus on examples of perovskites processed by each route and subsequently utilized in energy-related applications. Please refer to books and review articles for more detailed explanations of the sintering processes in general [20,21,23–26,28,29,68,70,71]. An overview of the three different sintering routes is given in Table 1 at the end of this section.

4.1. Solid-state sintering

The traditional solid-state sintering process – also denoted as conventional sintering – involves heating shaped powders at temperatures typically ranging from 0.5 to 0.9 of their respective melting points. During this process, atomic diffusion in the solid state leads to particle necking, reduction in porosity, and densification, followed by grain growth in the final stage [22]. Aside from densification and porosity reduction, solid-state sintering can significantly alter relevant properties for energy-related applications.

A variety of research groups worldwide have dedicated their research efforts to understand the morphological changes and microstructural evolution of perovskites depending on the sintering parameters [22,42,73,74]. Those involve investigations focused on the densification process, e.g., the numerical study by Ni *et al.* [75] simulated the solid-state sintering process of $MgTiO_3$ dielectric ceramics, as well as fundamental investigations to uncover microstructure-properties relationships. Bah *et al.* have monitored the sintering of piezoelectric $K_{0.5}Na_{0.5}NbO_3$ particles in situ, showing that the shrinkage was directly related to the grain boundary migration during sintering [3]. A detailed microstructural analysis performed by Han *et al.* [76] uncovered distinct cubic phases within different grains for $BaZr_{0.8}Y_{0.2}O_{3-\delta}$ and $Ba_{0.9}Zr_{0.8}Y_{0.2}O_{3-\delta}$, sintered at 1600 °C due to Ba-deficiency. Meanwhile, Shirpour *et al.* [77] reported Ba losses for $BaZrO_3$ samples sintered with very long dwell times of around 60 h, significantly reducing both volume and grain boundary conductivities. Stevenson *et al.* observed that $(La_{0.9}Sr_{0.1})_xGa_{0.8}Mg_{0.2}O_{3-\delta}$ and $(La_{0.8}Sr_{0.2})_xGa_{0.8}Mg_{0.2}O_{3-\delta}$, presented swelling due to volatilization of Ga_2O from the perovskite structure at 1550 °C [78]. Some of the scientific investigations aimed at mitigating undesirable effects such as partial phase evaporation, swelling, and uncontrollable or extensive grain growth [73,74].

For the fabrication of highly-dense bulk perovskites' components, elevated temperatures are imperative in the solid-state sintering method, with the undesirable effect of grain growth. Not only the mechanical properties, but also the electrical and magnetic properties of perovskite-type structures can be adversely affected by grain growth [24]. Consequently, several alternative methods have been proposed to attain fine microstructure and highly dense ceramics at lower temperatures.

Table 1
Summary of sintering routes including their requirements and process parameters.

Sintering route	Solid-state sintering	Liquid phase sintering	Spark plasma sintering
Setup requirements	Furnace with heating and atmosphere control	Furnace with heating and atmosphere control, additives for powder	Furnace with temperature and atmosphere control, graphite die and punches, DC power supply, pyrometer
Maximal temperature	~2000 °C	~1500 °C	2400 °C
Maximal Heating rates	~10 °C/min	~150 °C/min	1000 °C/min
Process duration	Several hours to days	Several hours	< 1 h to few hours
Microstructure	Grain coarsening, isolated pores evolution	Grain coarsening, pore elimination	Retains grain structure during densification
Ref.	[20,22,23]	[26,28,79]	[20,29]

4.2. Liquid phase sintering

One suggested approach to reduce sintering temperatures is to use sintering aids that form a liquid phase during heating, leading to liquid phase sintering [79]. The presence of small amounts of liquid leads to the rise of capillary forces that promote densification by allowing solid dissolution away from high-energy surface regions, followed by reprecipitation [26,80]. LPS can be classified into two groups, i.e., transient liquid phase sintering and persistent liquid phase sintering. In transient liquid phase sintering, the liquid remains present only in the early stages of sintering. In contrast, in the persistent liquid phase, the liquid phase remains present throughout the sintering process [71,80].

Recently, Charan *et al.* [81] fabricated $SrTiO_3$ with different additives (Al_2O_3, CuO, and ZnO) at varying concentrations (1–5 wt%) by liquid phase sintering. LPS enhanced the electrical conductivity of sintered components due to the higher densification. A modified liquid-phase-assisted sintering mechanism has been employed to enhance the sintering characteristics of $La_{0.8}Sr_{0.2}Cr_{1-x}Fe_xO_{3-\delta}$ used as an interconnect in solid oxide fuel cells. The prefabricated powder calcinated at 1000 °C was sintered using LPS at 1400 °C for 4 h. However, samples with lower Fe content ($x = 0.1$ and 0.2) exhibited shape distortion and irregular surface features indicative of an excess of liquid phase, negatively influencing the material's conductivity [82]. The latter study shows that albeit LPS enables densification at lower temperatures compared to solid-state sintering, it can present some disadvantages such as dimensional distortion, compromised mechanical properties due to solidification of brittle phases along grain boundaries, and restrictions in high-temperature applications and alloying element choices due to thermodynamic factors [26,71].

4.3. Spark plasma sintering

Many perovskites' compounds have been produced using spark plasma sintering (SPS) [83–86]. SPS is an advanced electrically activated/assisted technique that uses a pulsed electric current to generate resistive heating while applying a uniaxial mechanical load [20,68]. In the SPS process, the sample is placed under a controlled atmosphere (e.g., vacuum, air, or argon) within a mechanical system operating as a high-power electrical circuit and press [87].

The SPS method can synthesize new compounds and/or densify materials in a single step, eliminating the need for long periods at high temperatures, greatly simplifying the manufacturing process, and lowering costs. This technique provides improved control over the microstructure and composition, as it can aid in avoiding undesired reactions or excessive grain growth [28,29]. In this context, mitigating grain growth can significantly impact the performance of perovskite-based electrochemical devices, such as solid oxide fuel cells. Ricote *et al.* [88] reported that sintering $BaZr_{0.9}Y_{0.1}O_{3\text{-}\delta}$ using the SPS technique at 1700 °C for 5 min not only prevented barium evaporation but also resulted in a significant densification rate (99.8 %), improving the conductivity in comparison to earlier reports. Hence, the fuel cell efficiency for energy conversion is enhanced. Also, the sintering environment's composition and its constituents' partial pressure exert a significant influence on defect structure [89,90] and perovskite sintering diffusivity [29].

Moreover, SPS has been shown to impact other perovskite compounds' properties significantly [91–93]. For instance, SPS has proven effective in enhancing the electrical conductivity of $BaCe_{0.4}Zr_{0.5}Y_{0.1}O_{3\text{-}\delta}$ solid oxide fuel cell at lower temperatures (400–500 °C), compared to the traditional method [94]. Song *et al.* [92] also found that SPS can improve the ferroelectric, magnetic, and dielectric properties of $BiFeO_3$. Similarly, SPS has been explored to enhance the dielectric properties of $CaCu_3Ti_4O_{12}$ [90] and $BaTiO_3$ [95], resulting in improved electric breakdown fields and reduced dielectric loss, which are desirable attributes for energy applications. Overall, these findings highlight the versatility of SPS as a promising method of fabricating perovskite with superior properties, making it a valuable tool in energy transition and other technological advancements.

5. Applications in energy storage

Notably, perovskites have found substantial application as solar cells and photodetectors [96–98]. However, their unique properties also hold promise in the domain of energy storage. Recently, energy storage technologies have received a lot of attention because of the irregular availability of energy resources, which highlights the need for novel and efficient ways to store, capture, and release electrical power on demand [5,99,100]. Lithium-ion solid-state batteries, supercapacitors, and solid capacitors have emerged as the prevailing electrochemical energy storage devices [101,102]. The following sections depict the research of sinter-based perovskites for application in those distinct domains.

5.1. Capacitors

A conventional capacitor stores energy by static electricity through the polarization of a dielectric electrode material placed between the capacitor's plates. This polarization results in the accumulation of electric charges on opposing plates, generating an electric field between them [103]. The composition and properties of the dielectric material assume a pivotal role in determining the final performance of the device since there are limitations of solely increasing the size of the conductive plates to store a substantial amount of energy [104]. Against this background, the search for high-performance dielectrics has driven the research of perovskites as a component in capacitors for high-energy storage. Due to their varied chemical compositions and acceptance of doping described in Section 2, perovskites can be customized to have optimized electrical properties. This flexibility enables the development of perovskite capacitors, offering a wide range of dielectric constants due to their diverse crystalline forms [5,105–108]. In fact, one of the primary advantages of "capacitor-type" perovskites over other common dielectric materials, such as aluminum oxide (Al_2O_3), is their relatively higher dielectric constant (ε). A high dielectric constant allows capacitors to store more electric charge in a smaller volume [109,110]. This characteristic is particularly attractive for the development of compact capacitors, such as the ones employed in microelectronic devices [110, 111].

In this context, several studies report an increase in the dielectric constant with the sintering temperature [111–115]. The dielectric constant rise is generally associated with a space charge's polarization at the heterointerfaces between grains and grain boundaries [114,116]. However, dielectric loss can also be observed during high-temperature sintering, which is attributed to the loss of oxygen in the crystal lattice or additional defects that allow the conduction jump of electrons (multivalence, for example, Fe^{2+} and Fe^{3+} ions), making the grains more conductive [111,112]. Moreover, previous studies have shown that it is possible to increase the material's permittivity by optimizing their sintering. Through the sintering, it is possible to introduce relaxing behavior and control the grain size and density of the perovskites [117]. Sintering process parameters, predominantly temperature, significantly impact the resistivity and resilience of grain boundaries. Therefore, it is essential to carefully regulate and optimize the sintering process (temperature, time, atmosphere, and pressure) to produce the appropriate electrical properties. Table 2 provides a compilation of sintered perovskites employed as capacitors.

Some studies have highlighted the superior energy storage capacity of perovskite materials produced by novel sintering methods compared to conventional sintering. While solid capacitors are known for their high temperature stability and fast charge-discharge speed, their energy storage densities are relatively low [101,117]. Sintering at lower temperatures but with densification assured by SPS has been reported to obtain homogenous perovskite materials with a higher energy storage density (W) [121,135]. $CaTiO_3$ perovskite produced by SPS exhibited fine, uniform microstructures with a W of 6.9 J cm^{-3} and a higher dielectric strength (E_b) of 910 kV cm^{-1}, greatly overperforming the material produced via conventional sintering, which had a W of 1.5 J cm^{-3} and an E_b of only 435 kV cm^{-1115}. According to Wu *et al.* [121], SPS can also enhance the energy storage performance of $Ba_{0.3}Sr_{0.7}TiO_3$ (Fig. 4(A) and (B)).

In comparison, the material produced by conventional sintering presented a W of 0.57 J cm^{-3}, while the one produced via SPS had a much higher value of 1.13 J cm^{-3}. Regarding energy storage efficiency, these results show an improvement from 69.3 % to 86.8 % with SPS. A similar improvement in W was reported by Mishra *et al.* [119] in a complex perovskite (Na, Bi, Ba)$_{0.5}$(Ti, Fe)$_{0.5}O_3$, which presented values 0.77 J cm^{-3} and 1.37 J cm^{-3} for conventional sintering and SPS, respectively (Fig. 4(C) and (D)).

In general, the prospect of higher energy density is exciting.

Table 2
Summary of sintered perovskite oxides for application in capacitors. The following sintering methods are used for fabricating the perovskites: conventional sintering (CS), which is also denoted as SSS, sintering with hot pressing (HPS), SPS, LPS, and transformation superplastic sintering (TSS).

Material	Sintering method	W (J cm^{-3})	Ref.
$Ba(Mg_{1/3}Nb_{2/3})O_3$	CS	5.90	[5]
$\{Bi_{0.5}[(Na_{0.8}K_{0.2})_{0.90}Li_{0.10}]_{0.5}\}_{0.96}Sr_{0.04}(Ti_{0.975}Ta_{0.025})O_3$	HP	2.42	[118]
$BaBiFeTiO_6$	CS	6.01	[106]
(Na, Bi, Ba)$_{0.5}$(Ti, Fe)$_{0.5}O_3$	CS	0.77	[119]
	SPS	1.40	
$CaTiO_3$	SPS	6.90	[120]
$Ba_{0.3}Sr_{0.7}TiO_3$	SPS	1.37	[121]
	CS	0.57	
$BaTi_{0.85}Sn_{0.15}O_3$/MgO	SPS	0.51	[122]
$Ba_{0.4}Sr_{0.6}TiO_3$/MgO	SPS	1.50	[123]
$0.9(K_{0.5}Na_{0.5})NbO_3$–$0.1Bi(Mg_{2/3}Nb_{1/3})O_3$	LPS	4.02	[124]
$0.8(K_{0.5}Na_{0.5})NbO_3-0.2\ Sr(Sc_{0.5}Nb_{0.5})O_3$	LPS	2.60	[125]
$Na_{0.5}Bi_{0.5}TiO_3$	CS	1.91	[126]
$Sr_x(Bi_{1-x}Na_{0.97-x}Li_{0.03})_{0.5}TiO_3$ (x = 0.30)	CS	1.70	[127]
$Na_{0.46}Bi_{0.46}Ba_{0.05}La_{0.02}Zr_{0.03}Ti_{0.97}$-$Sn_xO_3$ (x = 0.03)	CS	1.53	[128]
$Bi_{0.5}Na_{0.5}TiO_{3\text{-}x}Sr_{0.7}Bi_{0.2}TiO_3$	CS	2.20	[129]
$Bi_{0.5}Na_{0.5}TiO_3$	TSS	2.74	[130]
$AgNbO_3$	LPS	6.10	[131]
$Ca_{0.5}Sr_{0.5}TiO_3$-SiO_2	CS	2.00	[132]
$SrTiO_3$	CS	1.86	[133]
$CaCu_3Ti_4O_{12}$	SPS	10.11	[134]
$Ba_{0.4}Sr_{0.6}TiO_3$	SPS	1.23	[121]

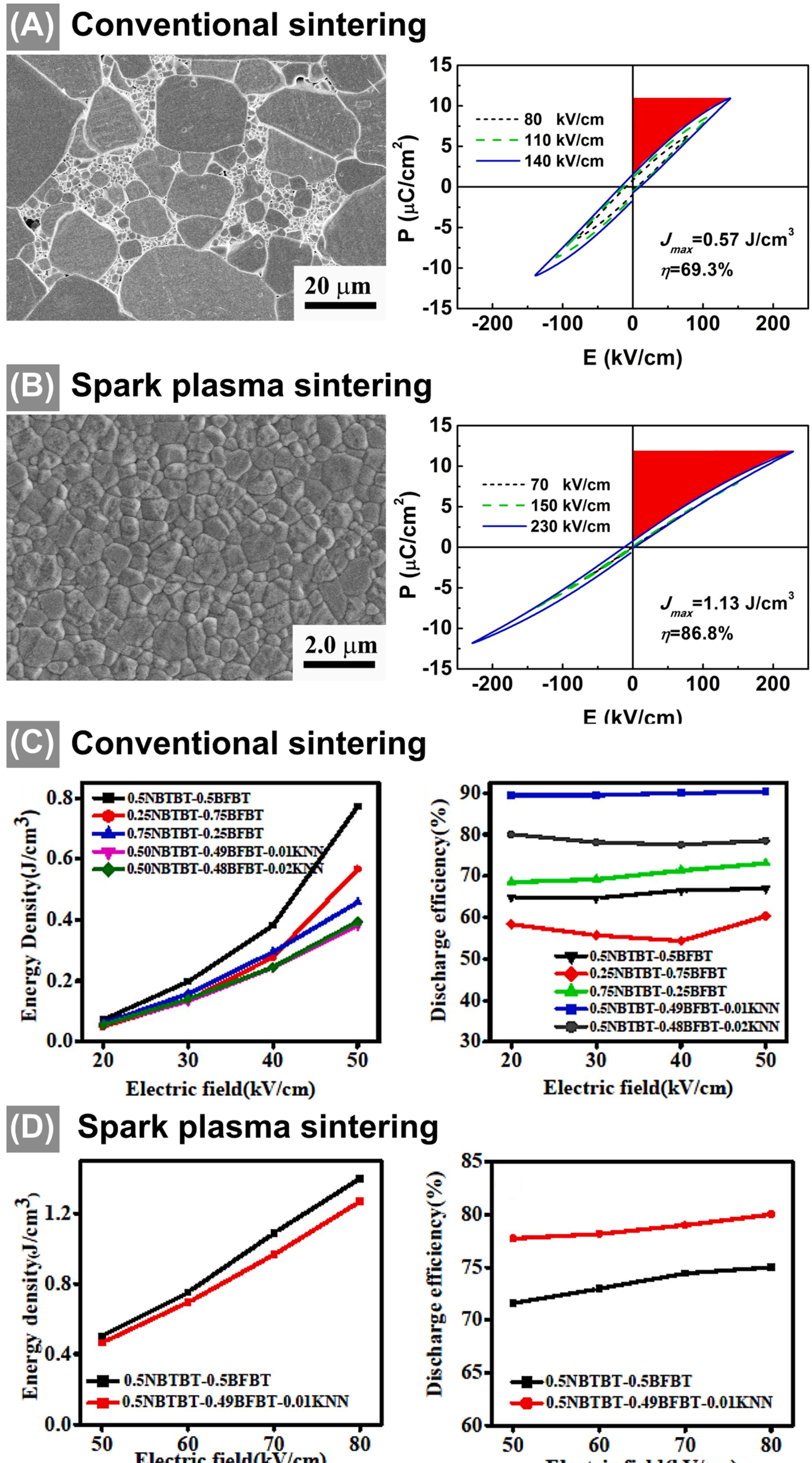

(caption on next page)

Fig. 4. Spark plasma sintering (SPS) improves the energy storage performance of perovskites compared to a sample prepared with conventional sintering (CS). (A and B) $Ba_{0.3}Sr_{0.7}TiO_3$ perovskites prepared by SPS feature higher energy density and discharge efficiency. Adapted with permission [121]. Copyright 2017, Elsevier. (C and D) The energy storage performance of $(Na, Bi, Ba)_{0.5}(Ti, Fe)_{0.5}O_3$ perovskites depends on their composition and the sintering process. The highest energy density is obtained for SPS samples fabricated from 50 % NBTBT (pseudo-binary alloy $0.8(Na_{0.5}Bi_{0.5}TiO_3)$-$0.2(BaTiO_3)$) and 50 % BFBT (pseudo-binary alloy $0.75BiFeO_3$-$0.25BaTiO_3$). This sample is denoted 0.5NBTBT-0.5BFBT. Doping with $K_{0.5}Na_{0.5}NbO_3$ (KNN) results in increased discharge efficiency. Figure adapted with permission [119]. Copyright 2017, Elsevier.

Improvements in their volumetric efficiency can significantly broaden the range of applications for capacitors, enabling easy integration, low cost, and miniaturization [136]. Further, by carefully choosing the sintering method and controlling the sintering parameters, researchers can optimize the perovskites' microstructure to improve their electrical properties and enhance their energy storage performance in capacitors [16,137].

5.2. Supercapacitors

Supercapacitors outperform traditional capacitors and batteries, representing a significant advancement in energy storage technology. They also have low internal resistance, a longer service life, and a wide application temperature range [138–140]. According to the principle of electrical energy storage, supercapacitors are divided into three groups. The first type is known as a double-layer electrical capacitor (EDLC). It relies on the charge-discharge (electrosorption) process in a double layer of electrical charges on porous electrodes separated by a monolayer of solvent molecules (molecular dielectric). EDLC is often composed of porous and spongy materials, such as carbon-based materials with a high specific surface area and good electrical conductivity [109,139–141]. Unlike EDLC, pseudocapacitors (PC) store electrical charge through oxidation-reduction (redox) reactions at the electrode-electrolyte interface and an intercalation mechanism, which allows ions to be adsorbed and desolvated within the electrode's structure. This system enables pseudocapacitors to improve overall capacitance, however producing less power density energy than EDLCs [141]. Transition oxides (MnO_2 and RuO_2), conductive polymers, and other redox-active materials can be used as electrode materials in pseudocapacitors. The last form is a hybrid system that combines the strengths of both EDLC and PC. Hybrid supercapacitors (HS) often comprise an asymmetric combination of a Li-doped graphite anode and an activated carbon cathode [104,109,139,141]. The choice of supercapacitor type depends on the specific requirements of each application, considering factors such as energy density, power density, life cycle, and cost-effectiveness. The energy storage capacitance of supercapacitors largely depends on the nature of the materials present.

Ongoing research focuses on optimizing and exploring chemical reaction mechanisms to develop novel electrode materials with high specific capacitance to enhance supercapacitor performance [140,142]. In this context, perovskite materials are widely recognized for their suitability as pseudocapacitance electrode materials, as the inclusion of multivalent cations in their structural framework facilitates redox reactions, which are imperative for pseudocapacitance charge storage [143,144]. Additionally, the capacity to intercalate and deintercalated ions within the crystal structure, or the introduction/increment of oxygen vacancies to uphold charge neutrality, holds substantial potential for improving pseudocapacitance and results in enriched energy density [143,145–147]. These approaches have been employed in several different perovskite compositions, namely $LaAlO_3$ [148], $SrCo_{0.9}Mo_{0.1}O_{3\text{-}\delta}$ [14] and $SrFe_xCo_{1\text{-}x}O_{3\text{-}\delta}$ [100], all focusing on utilizing the perovskite as an electrode in supercapacitors.

While the sintering process is widely used to improve dielectric capacitors' density and electrical resistivity [134,149], its application in supercapacitors is still in its infancy. This discrepancy is attributed to the distinct requirements of supercapacitors, namely, the imperative for high charge transfer rates and minimal electrical resistance, which can be adversely affected by conventional sintering techniques. However, Srither and Dhineshbabu [150] reported that the electrochemical properties of $FeTiO_3$ perovskite nanoparticles can be positively affected by low-temperature solid-state sintering. After sintering the material at 350 °C and 500 °C, the authors observed higher values of capacitance and discharge capacity (42 F g^{-1} and 129 mA hg^{-1}, respectively) for the samples sintered at higher temperatures in comparison to the ones sintered at 350 °C (22 F g^{-1} and 90 mA hg^{-1}). These differences result in a 50 % higher charge storage capacity associated with a longer lifetime. In addition, Karki and Ramezanipour [151] recently reported the synthesis and solid-state sintering of $Ca_3GaMn_2O_8$ and $SrCa_2GaMn_2O_8$ oxygen-deficient perovskites as supercapacitor. The as-fabricated symmetric PC cells presented a combination of a high energy density (10.69 Wh kg^{-1} for $Ca_3GaMn_2O_8$ and 1.23 Wh kg^{-1} for $SrCa_2GaMn_2O_8$) and a power density of 1400 W kg^{-1} for a current density of 0.5 A g^{-1}. Both materials have demonstrated excellent stability and structural integrity without collapse or phase transformation after 1000 charge-discharge cycles.

Furthermore, Chung *et al.* [152] used amorphous SiO_2 coating and SPS sintering to fabricate core-shell $BaTiO_3$ perovskite structures. The SPS facilitated the formation of a highly dense microstructure while maintaining SiO_2 in an amorphous state. This synergy yields a material exhibiting supercapacitor behavior characterized by low dielectric losses and high thermal stability. The reoxidation barrier and dielectric property conferred by the SiO_2 layer enable this behavior, which allows the reversible reduction of the Ti^{4+} core and the optimal balance of internal grain conductivity.

These recent works highlight the great potential of sinter-based perovskites for supercapacitors, with a compelling need for collaborative research and development efforts to unlock their full potential.

5.3. Batteries

Batteries are made of stacked cells that convert chemical energy into electrical energy [153]. Each cell consists of two electrodes, an anode and a cathode, separated by an electrolyte. When a battery is connected to an external circuit, a chemical reaction occurs at the electrodes, causing a flow of electrons from the anode to the cathode, creating an electric current that can power various devices [153,154]. Among the many battery technologies [153], lithium-ion batteries with liquid electrolytes are widely used in portable electronics and electric vehicles due to their excellent performance [99,155]. However, this type of battery presents low thermal stability and safety hazards attributed to its leakage probability and high flammability, including self-ignition. Moreover, adverse electrode interactions can cause overheating and even catastrophic chemical fires [99,155]. Batteries with solid-state electrolytes have gained considerable attention in recent years [156] to address these issues. They offer broader electrochemical stability and aid in mitigating risks due to their non-flammability nature, dramatically reducing the probability of thermal runaway events [99,156,157]. The ionic conductivity of solid conductors is an electrical property that generally determines the performance of an all-solid-state battery. Achieving high total ionic conductivity, ideally greater than 10^{-3} S $cm^{-1,}$ is imperative for any battery application. Perovskite-type Li-ion solid electrolytes, including $Li_{3x}La_{2/3-x}TiO_3$ [158] and (Li, Sr)(B', B")O_3 (B' = Zr, Hf, Ti, Sn, Ga, etc., B" = Nb, Ta, etc.) [96], have emerged as promising candidates due to their high capacity, high ionic conductivity and stable cycling [99,157,158].

In this context, sintering plays a fundamental role in optimizing ionic conductivity in perovskite materials by microstructural control. As recently reported by Lin *et al.* [159] and depicted in Fig. 5(A-C), the application of mechanical pressure (440 MPa) to a low-temperature FAST/SPS process could increase ionic conductivity in electrolytes of the $Li_{0.33}La_{0.55}TiO_3$ (LLTO) perovskite type to acceptable levels, from 5×10^{-6} S cm^{-1} to 7.7×10^{-6} S cm^{-1}. In contrast, the LLTO material obtained by the conventional sintering method (1200 °C for 10 h) presented improved ionic conductivity values of 1.3×10^{-4} S cm^{-1}. According to the authors, the increased total ionic conductivity of traditionally sintered perovskite is related to grain coarsening, which removes grain boundaries. Likewise, Wu *et al.* [160] have shown that smaller grain sizes in SPS-sintered $Li_{0.3}La_{0.57}TiO_3$ (LLTO) resulted in smaller conductivity accounting to 1.9×10^{-6} and 9.8×10^{-10} S cm^{-1} at 0 °C for grain sizes of 860 and 25 nm, respectively (Fig. 5(D and E)). This was associated with the fact that interfaces such as grain boundaries can hinder the flow of ions. A change in the perovskite composition was explored by Huang *et al.* [157] who employed solid-state synthesis and sintering at 1300 °C for 10 h to prepare $Li_3Sr_{7/16}Hf_{1/4}Ta_{3/4}O_3$, reporting a high density of 6.5 g cm^{-3} and an impressive total Li-ion conductivity of 3.8×10^{-4} S cm^{-1} at 25 °C, coupled with a notably low activation energy of 0.36 eV. Different authors have explored other sintering approaches aiming at improving ion conductivity, including hot pressing [161], cold sintering [162], flash sintering [163], microwave sintering [164], and sintering additives incorporation [157,165,166].

In addition to Li-ion solid-state batteries, perovskites also play a crucial role in developing metal-air batteries, which some researchers consider the future of energy storage technology [167,168]. These batteries are based on reactions between the metal component and the air, including oxygen reduction reaction (ORR) and oxygen evolution reaction (OER), which are crucial for the metal-air battery performance and efficiency [169]. Such reactions can occur at the air electrode interface, such as in Zn-air batteries, or at the cathode interface, such as in Li-air batteries [168,170,171]. Rechargeable metal-air batteries have several benefits, including lower costs, lower pollutant emissions, and high specific capacity and energy density [170,172]. Nevertheless, metal-air batteries also present significant limitations due to the same electrochemical oxygen reactions, such as delayed power response and high reaction overpotential [169,171,173,174]. As a result, current research focuses mainly on developing electrocatalysts that combine benefits such as low cost, high stability, and ideal activity for metal-air batteries to decompose discharge by-products [168,174]. In this context, perovskite oxides emerge as promising electrode candidates due to their high inherent activity, ability to adjust composition, and relatively simple synthesis [174–177]. Nonetheless, there are just a few studies regarding the application of sinter-based perovskite oxides in metal-air batteries. Recently, Christy *et al.* [178] investigated a $La_{0.6}Sr_{0.4}CoO_{3-\delta}$ (LSC) perovskite as the cathode in a zinc-air battery. Their study compares perovskites produced by conventional sintering (1000 °C) and intense pulsed light technology (PLT). PLT significantly improved the bifunctional catalyst's ORR and OER catalytic activity, surpassing more than twice that of conventionally sintered LSC. When applied as an air cathode, LSC-PLT showed stable performance for 200 cycles with a low voltage range (1.4 V). In comparison, LSC sintered by the conventional method shows stable performance for 64 cycles with a voltage range of ~ 1.1 V. However, a separate, in-depth study is required to understand the mechanism behind the enhanced performance of the PLT material.

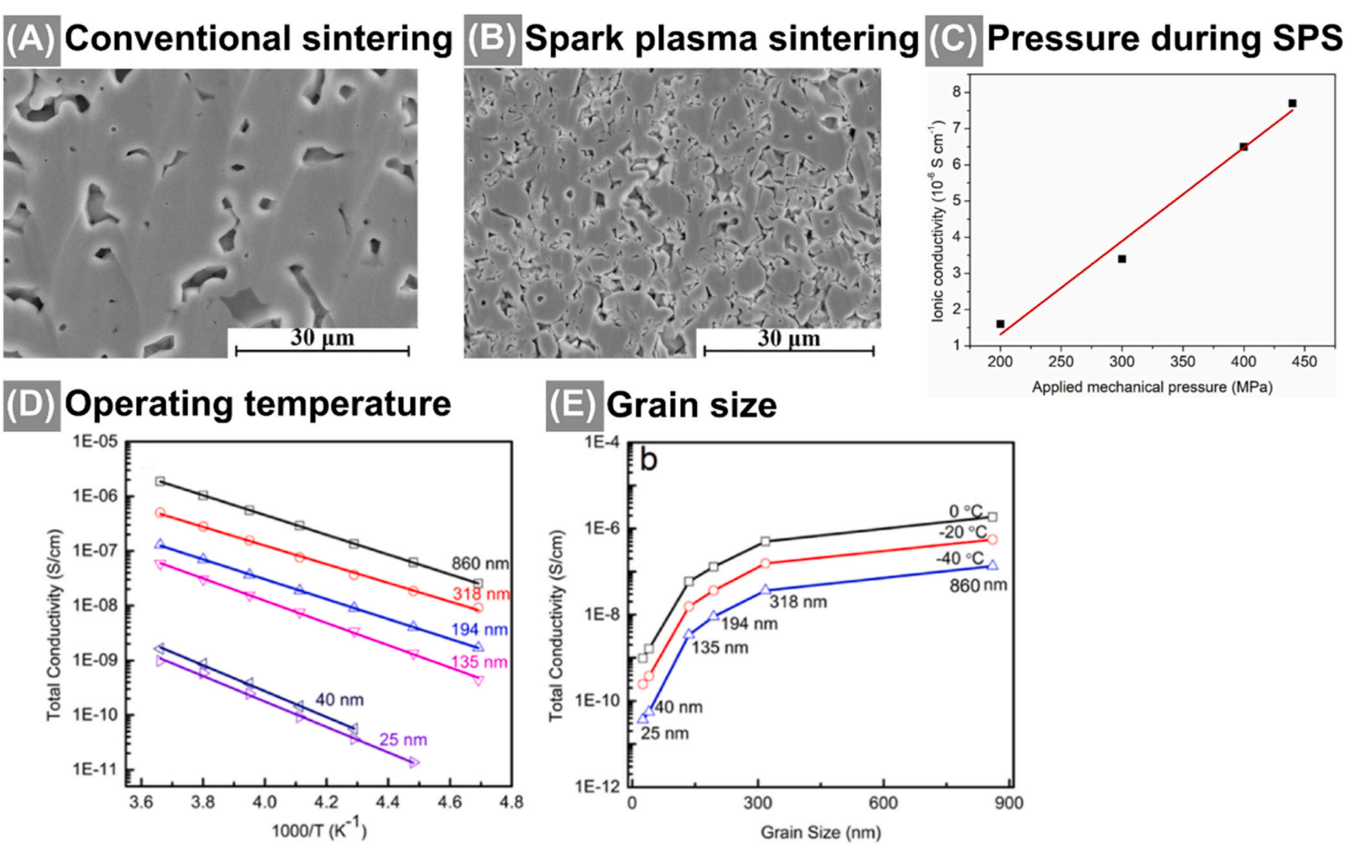

Fig. 5. Applications of sinter-based perovskites as battery electrodes are demonstrated for perovskite-type Li-ion solid electrolytes. (A-C) The microstructure of $Li_{0.33}La_{0.55}TiO_3$ perovskites is quite different depending on the sintering method, where samples sintered by (A) conventional sintering at 1200 °C for 10 h and (B) Spark plasma sintering (SPS) at 750 °C and 440 MPa for 10 min are shown. (C) SPS sintered samples reveal increased ionic conductivity with increasing applied mechanical pressure during sintering. Figures adapted with permission [159]. Copyright 2023, Elsevier. The performance of the sintered $Li_{0.30}La_{0.57}TiO_3$ perovskites also depends on (D) the operating temperature and (E) grain size. Figures adapted with permission [160]. Copyright 2017, Elsevier.

6. Applications in energy conversion and generation

6.1. Solid oxide fuel cells

Solid oxide fuel cells (SOFC) are electrochemical energy conversion devices with the potential to provide high conversion efficiency with minimal environmental impact, thus playing an essential role in sustainable energy generation [28,179]. A conventional fuel cell configuration comprises two electrodes (cathode and anode) separated by an electrolyte [179]. In SOFC, ceramic membranes presenting oxygen ion conductivity, such as Yttria-Stabilized Zirconia (YSZ), are utilized as a "solid" electrolyte to transport the electrically charged ions (O^{2-}) from the cell's cathode to the anode. There, the O^{2-} ions react with the fuel stored to release e^-, heat, and water; If hydrocarbon fuels are used, carbon dioxide is also released into the external circuit [179–181]. In theory, as long as reactants are delivered to the electrodes, power conversion is made possible by the fuel cell [179,181]. This electrochemical device can employ various power sources, from traditional hydrocarbons (methane, propane, or ethane) to the most modern formulations like hydrogen [180]. However, a conventional SOFC electrolyte must operate at about 800–1000 °C [182], which imposes significant challenges for the development of fuel cell technology. Such operation temperatures require not only considerable energy input, but also the use of rare, expensive materials as interconnectors [179,183].

To address the challenge of reducing their operating temperature, researchers continually explore new solutions in materials' compositions, membrane structure, or fuel cell design [182,184]. In this sense, developing novel electrolyte materials with high thermal and chemical stability, high corrosion resistance, and good oxygen conductivity holds promise to optimize SOFC performance [183,185]. Among the materials that meet the criteria, perovskite-type oxides (single-phase, composite, and complex heterostructures) have demonstrated outstanding performance and durability as SOFC electrolyte membranes at different temperature levels [186–188]. For example, solid electrolytes based on $BaCeO_{3-\delta}$ have presented good electrical properties [183,189], where the partial substitution of Ce with other elements, such as Zr [190,191], Nb, Y [192], or In [193], has notably improved their chemical stability against CO_2 and H_2O. Additionally, these substitutions can mitigate the decrease in ionic conductivity with decreasing operation temperature [192,194–196]. For example, Taillades *et al.* [197] synthesized doped perovskite powders of $BaCe_{0.7}Zr_{0.1}Y_{0.1}Yb_{0.1}O_{3-\delta}$ via flash combustion method, followed by solid-state sintering at 1300 °C to generate the electrolyte membranes. The SOFC mounted with this membrane showed superior performance, achieving a maximum power density of 634 mW cm^{-2} at 700 °C. As shown in Table 3, other sinter-based perovskite electrolytes have been considered for low-temperature applications [198,199]. In recent studies, Strontium-based perovskite electrolytes have also been explored for SOFC applications, showing great potential for lower application temperatures. Significant progress has been made by Shah *et al.* [200], where solid electrolytes of solid-state sintered Fe-doped $SrTiO_{3-\delta}$ (STO) perovskite have presented ionic conductivity of 0.17 S cm^{-1} with a power density of 540 mW cm^{-2} for SOFC operating temperature of 520 °C. In another study, the authors have investigated the substitution of Fe by Nb in the STO composition, further increasing the ionic conductivity and power density to 0.22 S cm^{-1} and 678 mW cm^{-2}, respectively [201]. Furthermore, the study conducted by Zainon *et al.* [42] delved into the influence of sintering temperature on the physical, electrical, and electrochemical properties of $La_{0.6}Sr_{1.4}MnO_4$ double perovskite anode films. The highest electrical conductivity was reached when the anode films were solid-state sintered at 1300 °C. This outcome was attributed to enhanced film densification, reduced porosity, and enlarged grain dimensions. Conversely, the most favorable electrochemical performance was observed in the film sintered at much lower temperature of 1000 °C, exhibiting an Area Specific Resistance (ASR) of 1.52 Ωcm^2. The authors associated this superior electrochemical performance with the larger film thickness of the samples sintered at lower temperatures, facilitating the hydrogen oxidation reaction.

Furthermore, sinter-based oxide perovskites can also be used as a cathode material in SOFC. Some critical aspects of SOFC cathodes include having good catalytic activity, thermodynamic stability, and compatibility with the electrolyte [203]. Regarding electrochemical performance, cobalt-containing perovskites have been identified as a promising cathode material due to their high oxygen ion diffusivity and electrical conductivity for ORR [187,188,204]. Recently, Baek *et al.* [188] investigated the impact of varied solid-state sintering temperatures (1000–1150 °C) on the electrocatalytic properties of $SmBa_{0.5}Sr_{0.5}Co_2O_{5+\delta}$ (SBSCO) SOFC cathode material. As shown in Fig. 6(A-B), their study indicates a direct correlation between sintering temperature and electrical conductivity, highlighting a significant increase of conductivity of SBSCO from 215.27 S cm^{-1} at 1000 °C to a peak of 772.68 S cm^{-1} at 1150 °C. The associated microstructural analysis results revealed that the sintering temperature of 1150 °C led to an increase in grain size, which shortened the charge carrier pathways and thus increased conductivity. Such results emphasize the critical influence of sintering conditions on perovskite electrocatalytic performance, where aspects often seen as detrimental (such as grain growth), actually could be used to optimize the SOFC performance.

Other perovskites compositions have been explored as cathode material, where different authors have reported low operation temperatures in the 600–800 °C range [203,206,207]. The SOFC containing $La_{1.4}Ca_{0.6}CoMnO_{5+\delta}$ as a cathode material reported by Li *et al.* presented conductivity values ranging between 166 and 228 S cm^{-1} for low operation temperatures between 600 and 850°C. Notably, the SOFC showcased a remarkable conversion efficiency of 543 mW cm^{-2} at 800 °C, utilizing H_2 as the fuel and oxygen as the oxidant [203]. Yang *et al.* [207] also reported the excellent power density of 625 mW cm^{-2} at 700 °C for an SOFC with $Sr_{0.95}Ce_{0.05}CoO_{3-\delta}$ as cathode material. Despite their remarkable performance, perovskites containing Co ion substitution exhibit severe chemical stability issues and thermal tension between cell components [208,209].

Furthermore, the high cost of cobalt associated with the potential

Table 3
Performance comparison of perovskite electrolytes in SOFC at various temperatures.

Electrolyte	Sintering method	Operating temperature (°C)	Conductivity (S cm^{-1})	Conversion efficiency (mW cm^{-2})	Ref.
$Ba_{0.5}Sr_{0.5}Ce_{0.6}Zr_{0.2}Gd_{0.1}Y_{0.1}O_{3-\delta}$	SSS	850	-	1000	[195]
$BaCe_{0.7}Zr_{0.1}Y_{0.1}Yb_{0.1}O_{3-\delta}$	Co-sintering	700	-	634	[197]
$BaZr_{0.1}Ce_{0.7}Y_{0.1}Yb_{0.1}O_{3-\delta}$	Microwave sintering	700	0.038	640	[202]
$BaCe_{0.8}Y_{0.1}Ni_{0.04}Sm_{0.06}O_{3-\delta}$	SSS	650	0.01	-	[192]
$BaCe_{0.85-x}Y_{0.15}NixO_{3-\delta}$	SSS	600	0.01	-	
$BaCe_{0.7}In_{0.2}Yb_{0.1}O_{3-\delta}$	Co-sintering	600	0.0027	218	[193]
$BaCo_{0.2}Fe_{0.1}Ce_{0.2}Tm_{0.1}Zr_{0.3}Y_{0.1}O_3$	SSS	530	0.193	661	[191]
Fe-$SrTiO_{3-\delta}$	SSS	520	0.17	540	[200]
Nb-$SrTiO_{3-\delta}$	SSS	520	0.22	678	[201]
$La_{0.9}Sr_{0.1}Ga_{0.8}Mg_{0.2}O_{3-\delta}$	SSS	800	223	445	[203]
$La_{0.6}Sr_{1.4}MnO_4$	SSS	800	3.73	-	[42]

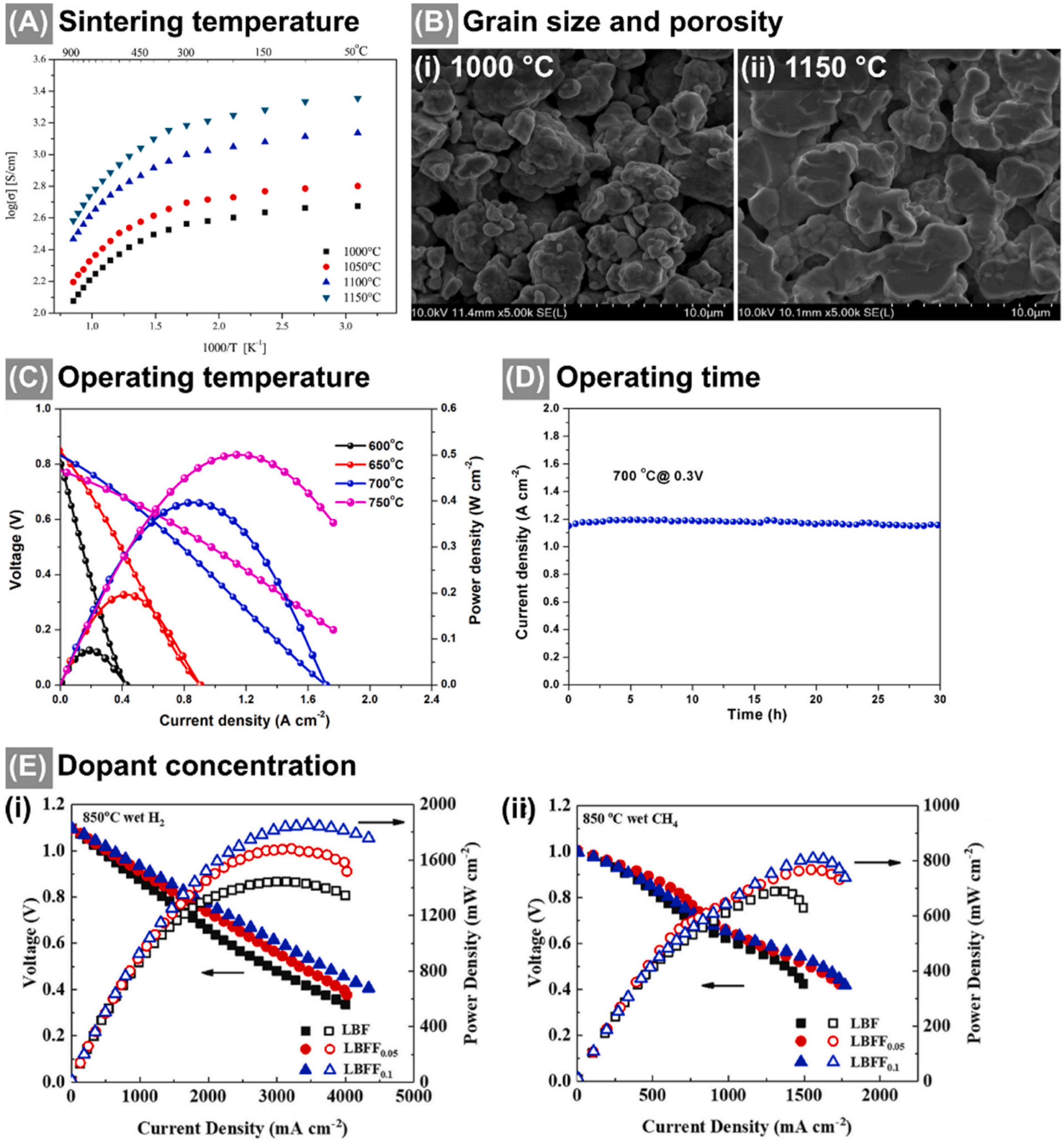

Fig. 6. Various sinter-based perovskites are applied as cathodes or anodes in SOFCs. (A-C) $SmBa_{0.5}Sr_{0.5}Co_2O_{5+\delta}$ cathodes reveal a significant influence of the sintering temperature on their performance shown in (A), which is associated with different microstructures shown in (B). Figures adapted with permission [188]. Copyright 2022, Elsevier. (C and D) A cobalt-free perovskite cathode consisting of $BaFe_{0.9}Nb_{0.1}O_{3-\delta}$ features an adequate electrochemical performance (C) at different operating temperatures and (D) over 30 h operation time. Figures adapted with permission [187]. Copyright 2021, Elsevier. (E) Fluor doping of $La_{0.5}Ba_{0.5}FeO_3$ (LBF) anodes improves the activity and stability of SOFCs utilizing (i) wet H_2 and (ii) wet CH_4 as fuels. The doped perovskite materials are denoted as $LBFF_x$, where x displays the F content. Figures adapted with permission [205]. Copyright 2022, Elsevier.

environmental toxicity negatively affects the commercial attractivity of the material [210]. To overcome these challenges, scientists have been exploring alternative elements. Among them, Ferrite-containing perovskite has been considered a more sustainable option [211], since sintered materials such as $La_{0.5}Sr_{0.5}Fe_{0.9}Mo_{0.1}O_{3-\delta}$ [212], $La_{1.2}Sr_{0.8}Ni_{0.6}Fe_{0.4}O_{4+\delta}$ [213], $La_{0.5}Ba_{0.5}Cu_xFe_{1-x}O_{3-\delta}$ [214], and $BaFe_{0.95}Nb_{0.05}O_{3-\delta}$ [215] exhibit high electrochemical properties. Recently, Wang *et al.* [187] prepared a promising cobalt-free perovskite cathode composition, $BaFe_{0.9}Nb_{0.1}O_{3-\delta}$, that shows reasonably electrochemical performance (Fig. 6(C and D)). In detail, the performance is evidenced by the polarization resistance of 0.102 Ω cm^{-2} and the peak power density of 397 mW cm^{-2} using H_2 as fuel and ambient air as oxidant at 700 °C without significant degradation in cell performance detected over 30 h.

Sinter-based perovskites have also been extensively researched as possible SOFC anode materials. Similar to the basic requirements for cathodes, a suitable anode material should have high catalytic activity to achieve a high level of electrochemical oxidation of fuel under SOFC operating conditions [216]. Sinter-based perovskites composed of Cr, Ti, Ga, and Mn appear promising [17,204,217,218]. For example, Xia *et al.* [219] manufactured $La_{0.57}Sr_{0.15}TiO_3$ perovskite under different solid-state sintering conditions. The results indicate that the optimum temperature for sintering to provide a good contact between anode and electrolyte was 1250 °C with an associated polarization resistance of 0.73 Ω cm^{-2} at 800 °C for 3 % H_2O/H_2. Interesting results have been obtained with another conventional composition for SOFC: $La_{0.5}Sr_{0.5}Fe_{0.9}Mo_{0.1}O_{3-\delta}$. A superior cell performance was achieved where maximum power densities of 722 mW cm^{-2} and 513 mW cm^{-2} were measured at 800 °C operating temperature when using H_2 and CH_4, respectively [220]. Recently, Hou *et al.* [205] synthesized a $La_{0.5}Ba_{0.5}FeO_3$ anode with a $La_{0.8}Sr_{0.2}Ga_{0.8}Mg_{0.2}O_3$ electrolyte layer and achieved power densities of 1446 and 691 mW cm^{-2} at 850 °C using wet H_2 and CH_4 as fuels, respectively (Fig. 6(E)). In addition, they tested the incorporation of F into the $La_{0.5}Ba_{0.5}FeO_3$ structure, which enhanced catalytic activity and led to a remarkable rise in power densities of 1860 and 809 mW cm^{-2} at similar conditions.

6.2. Solid oxide electrolyte cells

Solid Oxide Electrolysis Cells (SOECs) are advanced electrochemical devices that play an important role in energy generation and storage, particularly in the context of sustainable energy [221,222]. These devices are regarded as a promising technology to produce clean fuels, reduce CO_2 emissions, and enable large-scale energy storage [221,223]. A SOEC is composed of three main components (electrolyte, oxygen electrode, and fuel/hydrogen electrode) that, combined with a power source, can electrochemically split steam and CO_2 into H_2 and CO or convert an H_2O-CO_2 mixture into synthesis gas (syngas; H_2 and CO) [221,224,225]. SOECs are under continuous development, and previous studies have focused on improving cell components in terms of durability, electroactivity, and selection of alternative materials to reduce device costs. Similar to SOFCs, a perovskite electrolyte with high ionic conductivity and negligible electronic conductivity could be applied to SOECs. $La_{1-x}Sr_xGa_{1-y}Mg_yO_{3-\delta}$ (LSGM) sintered perovskite is a recurrent composition researched as potential SOEC electrolyte for H_2 production. Recently, Kim *et al.* [226] investigated a combination of LSGM-sintered electrolytes with a sonic spray approach. During electrochemical electrolysis at 800 °C and 1.3 V, the cell attained a current density of 1.15 A cm^{-2} and a high ionic conductivity of 0.1 S cm^{-1}. Table 4 presents an overview of reported electrolysis current densities of a few possible LSGM sintered perovskite investigated as SOEC electrolytes. Despite its outstanding performance, the LSGM can exhibit chemical incompatibility with nickel, the usual material used in fuel electrode composition (Ni-YSZ), and Ga^{3+} to Ga^{2+} reduction [227].

Therefore, hydrogen production requires more stable materials. Proton-conducting perovskites, such as doped $BaCeO_3$ and $BaZrO_3$, are interesting candidates for application in SOEC because of their high conductivity and stability [183,235–237]. The $BaZr_{0.1}Ce_{0.7}Y_{0.1}Yb_{0.1}O_{3-\delta}$ (BCZYYb) perovskite composition has been widely adopted to combine both properties. However, $Ba(Zr,Ce,Y,Yb)O_{3-\delta}$ often requires a long dwell time at high temperatures and assisted sintering to obtain high densification (>94 %) [238–240]. Unfortunately, high sintering temperatures can affect the composition of the material due to Ba evaporation, segregation of doped cations, and undesirable reactions with the electrode [183,240,241]. Hence, flash sintering [238], spark plasma sintering [94], and using sintering aids, such as liquid phase sintering, have been investigated to promote densification at lower sintering temperatures [237,239,240].

Another challenging but necessary step toward improving the SOEC's catalytic performance is the development of novel electrode materials. Several sintering processes, including solid-state sintering [242–245], spark plasma sintering [246], and microwave-assisted sintering [247,248], have been employed to consolidate perovskites SOEC electrodes. Sintering conditions, in particular temperature, can influence the cell components' microstructure and polarization resistance (Rp) [249–252]. Some recent advancements on sintered perovskite for SOEC include the development of solid-state sintered $Ba_{0.95}La_{0.05}FeO_{3-\delta}$ as an oxygen electrode by Yang *et al.* [253]. In CO_2 electrolysis, the material achieved current density of 1.11 and 2.42 A cm^{-2} under 1.5 V and intermediate temperatures of 700 and 800 °C, respectively. At the same temperature range, the electrolysis current density was between 0.85 and 1.53 A cm^{-2} under 50 %H_2–50 %CO_2 conditions. Overall, the cell's stability performance was assessed for over 200 h with no detectable degradation. Also, Li *et al.* [254] prepared a promising perovskite material for SOEC oxygen electrode at low solid-state sintering temperature of 1100 °C (Fig. 7(A)). The samples comprised of $Pr_{0.6}Ca_{0.4}FeO_{3-\delta}$ showed a current density of 277.14 mA cm^{-2}, which corresponds to a hydrogen production rate of 115.84 mL cm^{-2} h^{-1} at 800 °C under 1.3 V. Furthermore, following a 10-hour short-term stability test, the air electrode showed strong stability with no evidence of delamination.

Similar to the oxygen electrode, the fuel/hydrogen electrode is a porous structure that must permit rapid mass transport of steam and product gases (H_2). As previously stated, Ni/YSZ is commonly used as a fuel electrode of oxygen-ion SOEC due to its availability and affordable cost. Unfortunately, Ni/YSZ cermets can show signs of degradation and suffer delamination at higher current levels (1.5 A cm^{-2}), which lowers cell performance [227]. Sintered perovskites, such as $La_{1-x}Sr_xCr_{1-y}Mn_yO_3$ [243,256], $La_{1-x}Sr_xTiO_3$ [257], and $La_{1-x}Sr_xCr_{1-y}Fe_yO_3$, [258] have been investigated as alternate fuel electrodes due to their high electronic conductivity, low polarization resistance, and chemical stability. In addition, Teng *et al.* [254] reported a successful case of solid-state sintered oxide electrolysis cells using $La_{0.4}Sr_{0.55}Co_{0.2}Fe_{0.6}Nb_{0.2}O_{3-\delta}$ hydrogen electrode (Fig. 7(B-D)). The introduction of A-site cation deficiency into the perovskite oxide lattice promoted the exsolution of Co and Fe. As a result, high water electrolysis was observed, and the cell produced 399 mL $cm^{-2}h^{-1}$ of hydrogen, corresponding to a current density of 0.956 A cm^{-2} under 1.3 V at 850 °C.

Table 4
Comparison of electrolysis performance of the various SOECs at 1.3 V.

Electrolyte	Sintering method	Cell configuration	Test condition	Current density (A cm^{-2})	Refs.
$La_{1-x}Sr_xGa_{1-y}Mg_yO_{3-\delta}$	Co-sintering	NiO-GDC/ LDC /LSGM/ SSC	50 % H_2O, 50 % H_2, 800 °C	1.15	[226]
	Co-sintering	NiO-Y_2O_3/ ZrO_2/ LSGM/ SSC	10 % H_2, 50 % CO_2, 40 % Ar, 800 °C	1.682	[228]
	SSS	SFM/ LSGM/ SFM	40 % H_2O, 60 % H_2, 800 °C	0.48	[229]
	SSS	SFMNi-SDC/ LCO/ LSGM/ SDC-LSCF	42 % H_2O, 58 % H_2, 850 °C	1.26	[230]
$Ba(Zr,Ce,Y,Yb)O_{3-\delta}$	Co-sintering	PBSCF-BZCYYb/ BZCYYb/ NiO-BZCYYb/ PBSCF-BZCYYb55	40 % H_2O, 60 % Air, 650 °C	0.744	[231]
	SSS	PNO/LCO/ BCZYYb/ BCZYYb-Ni	60 % H_2O, 40 % Air, 600 °C	0.330	[232]
	SSS		60 % H_2O, 40 % Air, 700 °C	0.975	
	SSS	PBSCF(PLD-modified)/ BCZYYb4411/ BCZYYb4411-Ni	3 % H_2O, 97 % Air, 600 °C	1.80	[233]
	SSS	SLF/ BCZY53/ BCZY53-Ni	20 % H_2O, 80 % Air, 700 °C	1.08	[234]

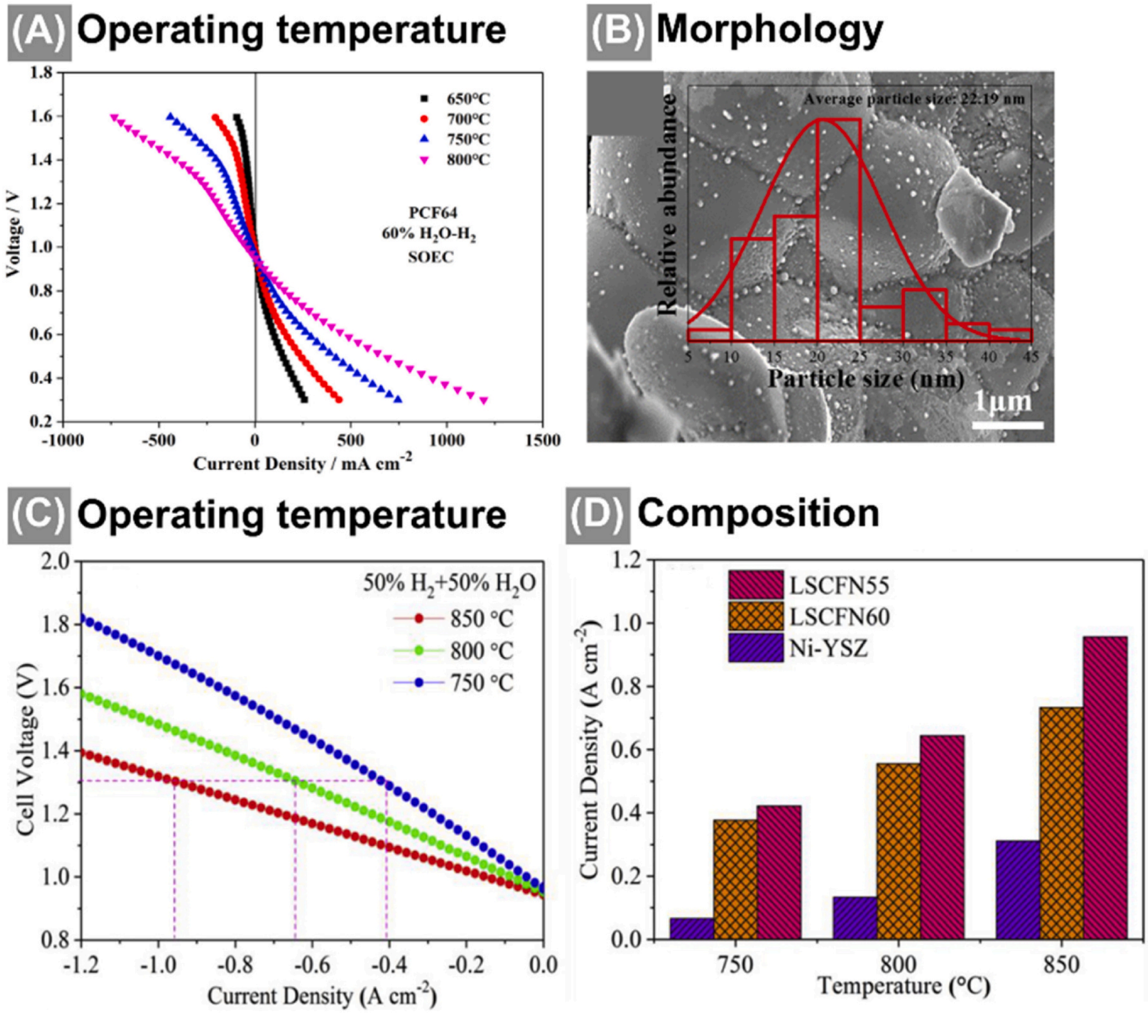

Fig. 7. Sinter-based perovskites demonstrate promising performances for application in SOECs. $Pr_{0.6}Ca_{0.4}FeO_{3-\delta}$ oxygen electrodes exhibit increased current density according to the operation temperature as depicted in (A). Figure adapted with permission [254]. Copyright 2021, Elsevier. (B-D) A-site cation-deficient $La_{0.4}Sr_{0.55}Co_{0.2}Fe_{0.6}Nb_{0.2}O_{3-\delta}$ (LSCFN) hydrogen electrodes show good water electrolysis results associated with the exsolution of Co_2Fe alloy nanoparticles, which are visible in the SEM image shown in (B). The material reveals high current densities at different operating temperatures (C) and outperforms conventional Ni-YSZ electrodes, as shown in (D). Figures adapted with permission [255]. Copyright 2020, Elsevier.

Overall, continued research and optimization of perovskite sintering techniques will lead to further advancements in energy technology, bringing SOEC closer to a sustainable and renewable energy future.

7. Summary and perspectives

This review highlighted the impact of sinter-based perovskites on advancing energy-related applications. The versatile structure of perovskites enables a wide range of cation substitutions, resulting in properties' tunability and unique physicochemical properties. This range of structural flexibility renders the utilization of perovskites in various energy-related applications, with this review covering applications ranging from energy storage solutions to energy generation and conversion techniques.

We have shown that such structural flexibility can be achieved already at the powder synthesis step, in which sol-gel chemistry, solid-state reactions, and hydrothermal methods are typically employed. For sinter-based perovskites – the main topic of this review – further properties' tunability can be achieved by choosing a sintering method or optimizing the sintering parameters such as atmosphere, time, and temperature. It has been shown that solid state and liquid phase sintering are employed among all the covered application fields. Furthermore, we have observed that spark plasma sintering is an emerging technique for fabricating perovskites, as it offers precise control over microstructure and composition, helping avoid unwanted reactions or excessive grain growth. The reviewed research demonstrated that the utilization of SPS can improve properties such as the perovskites' electrical conductivity, ion, and electron transport, making it a promising method for advancing energy-related applications. Energy storage applications of perovskites include their use in capacitors, solid-state batteries, and supercapacitors and approaches to use sinter-based perovskites are summarized in Table 5. The high dielectric constants of perovskites make them ideal for capacitors, while their structural adaptability increases their suitability for charge storage in supercapacitors. In energy conversion, perovskites promise significant improvements in SOFCs and SOECs as they serve as effective electrolytes and potential replacement materials for cathodes and anodes due to their excellent ionic conductivity.

Sinter-based perovskites are expected to play a crucial role in expanding energy applications in the future. Further advanced sintering techniques will enable greater control over perovskite microstructures, leading to improved efficiency and stability of devices. Efforts to improve ionic conductivity and interfacial stability through advanced microstructural design strategies should be prioritized to enable the integration of perovskites into compact, high-energy density devices. Further studies of new perovskite compositions – particularly those that

Table 5
Overview of sample requirements for different energy-related applications and properties of sinter-based perovskites prepared with different sintering routes.

Application	Sample requirements	SSS	LPS	SPS
Capacitors	High dielectric constant	Increased dielectric constant with sintering temperature; dielectric loss caused by sintering-induced defects; low to intermediate energy storage density	Intermediate energy storage density	Uniform microstructure; few defects; intermediate to high energy storage density
Supercapacitors	Depending on type; porosity; high charge transfer rates; ion intercalation; minimal electrical resistance	Increased capacity, discharge capacitance, and lifetime by low sintering temperature	Not reported	Dense microstructure; amorphous coating retains phase; low dielectric loss; high temperature stability
Batteries	High electric/ ionic conductivity	high ionic conductivity due to grain coarsening	Not reported	Ionic conductivity improvement when grains are large
Solid oxide fuel cells	Oxygen conductivity; high thermal and chemical stability; corrosion stability	High ionic conductivity by doping; enhanced densification and grain coarsening	Not reported	Not reported
Solid oxide electrolyte cells	High ionic conductivity; negligible electric conductivity	High ionic conductivity due to grain coarsening; improved stability	Higher densification at low sintering temperatures	Not reported

are cobalt- and lead-free or that contain environmentally friendly elements – could pave the way for cost-effective, sustainable energy solutions. In this regard, the exploitation of complex or high-entropy perovskites offers many opportunities, however, it is associated with the challenge of single phase formation and phase stability during application. In energy conversion, perovskites can further optimize SOFC and SOEC technologies, which could reduce costs and expand the use of alternative fuels such as hydrogen. Future research should focus on improving perovskites' electrochemical performance and longevity under real-world conditions while ensuring scalable manufacturing processes. Moreover, interdisciplinary research is required to overcome the inherent challenges and fully realize the potential of sinter-based perovskites to establish them as key components for sustainable energy technologies.

CRediT authorship contribution statement

González Sergio Y. G.: Writing – review & editing, Project administration, Formal analysis, Conceptualization. **Furlan Kaline Pagnan:** Writing – review & editing, Supervision, Resources, Project administration, Funding acquisition, Formal analysis, Conceptualization. **Carina Hedrich:** Writing – review & editing, Writing – original draft, Formal analysis. **Stefane V. Besegatto:** Writing – original draft, Formal analysis.

Declaration of Competing Interest

The authors declare that they have no known competing financial interests or personal relationships that could have appeared to influence the work reported in this paper.

Acknowledgements

The authors gratefully acknowledge the financial support from the German Academic Exchange Service (DAAD) and the Coordination for the Improvement of Higher Education Personnel (CAPES foundation) in the framework of the German-Brazilian bilateral research projects "Advanced nanostructured materials for sustainable pollutant abatement and energy production" project ID 57598489 and "Development of catalytic materials systems for non-intermittent green hydrogen production" project ID 57680884. Hedrich and Furlan also acknowledge TUHH's funding under the ID HEXC312003.

References

[1] S.A. Ali, T. Ahmad, Treasure trove for efficient hydrogen evolution through water splitting using diverse perovskite photocatalysts, Mater. Today Chem. 29 (2023) 101387, https://doi.org/10.1016/J.MTCHEM.2023.101387.
[2] E.A.R. Assirey, Perovskite synthesis, properties and their related biochemical and industrial application, Saudi Pharm. J. 27 (6) (2019) 817–829, https://doi.org/10.1016/J.JSPS.2019.05.003.
[3] M. Bah, R. Podor, R. Retoux, F. Delorme, K. Nadaud, F. Giovannelli, I. Monot-Laffez, A. Ayral, Real-Time capturing of microscale events controlling the sintering of Lead-Free piezoelectric Potassium-Sodium niobate, Small 18 (18) (2022), https://doi.org/10.1002/SMLL.202106825.
[4] J. Zhou, H. Zhang, A. Chang, Y. Zhao, Bi volatilization and conduction mechanism of rapidly liquid phase sintering La-Doped BiFeO3 perovskite ceramics, Journal Materials Science Materials Electronics 31 (12) (2020) 9595–9604, https://doi.org/10.1007/s10854-020-03502-8.
[5] R.D. Shi, X. Ma, P.P. Ma, X.L. Zhu, M.S. Fu, X.M. Chen, Ba-based complex perovskite ceramics with superior energy storage characteristics, J. Am. Ceram. Soc. 103 (11) (2020) 6389–6399, https://doi.org/10.1111/jace.17370.
[6] M. Zhou, R. Liang, Z. Zhou, C. Xu, X. Nie, X. Chen, X. Dong, High energy storage properties of (Ni1/3Nb2/3)4+ Complex-Ion modified (Ba0.85Ca0.15)(Zr0.10Ti0.90)O3 ceramics, Mater. Res. Bull. 98 (September 2017) (2018) 166–172, https://doi.org/10.1016/j.materresbull.2017.10.005.
[7] K. Karuppaiah, A. Raja, P.K. Ojha, G. Gurusamy, A.M. Ashok, Enhanced electrical properties of Ba6K2(Ca4Nb4)O21 complex perovskite oxide through modified sintering techniques, Materials Science Engineering B 246 (December 2017) (2019) 53–61, https://doi.org/10.1016/j.mseb.2019.05.027.
[8] E. Da Rosa Silva, M. Curi, J.V. Nicolini, J.G. Furtado, A.R. Secchi, H.C. Ferraz, Effect of doping concentration and sintering atmosphere on the microstructural and electrical characteristics of Y-Doped SrTiO3 perovskite anode for SOFC, Ceram. Int. 47 (10) (2021) 13331–13338, https://doi.org/10.1016/j.ceramint.2021.01.189.
[9] H. Tanaka, M. Misono, Advances in designing perovskite catalysts, Curr. Opin. Solid State Mater. Sci. 5 (5) (2001) 381–387, https://doi.org/10.1016/S1359-0286(01)00035-3.
[10] E. Grabowska, Selected perovskite oxides: characterization, preparation and photocatalytic Properties-A review, Appl. Catal. B Environ. 186 (2016) 97–126, https://doi.org/10.1016/j.apcatb.2015.12.035.
[11] A.E. Magdalin, P.D. Nixon, E. Jayaseelan, M. Sivakumar, S.K.N. Devi, M.S. P. Subathra, N.M. Kumar, N. Ananthi, Development of Lead-Free perovskite solar cells: opportunities, challenges, and future technologies, Results Eng. (2023) 101438, https://doi.org/10.1016/J.RINENG.2023.101438.
[12] G.R. Monama, K.E. Ramohlola, E.I. Iwuoha, K.D. Modibane, Progress on perovskite materials for energy application, Results Chem. 4 (2022) 100321, https://doi.org/10.1016/J.RECHEM.2022.100321.
[13] C. Moure, O. Peña, Recent advances in perovskites: processing and properties, Prog. Solid State Chem. 43 (2015) 123–148, https://doi.org/10.1016/j.progsolidstchem.2015.09.001.
[14] L. Zhu, R. Ran, M. Tadé, W. Wang, Z. Shao, Perovskite materials in energy storage and conversion, AsiaPac. J. Chem. Eng. 11 (2016) 338–369, https://doi.org/10.1002/apj.2000.
[15] S. Yan, C.H. Yim, V. Pankov, M. Bauer, E. Baranova, A. Weck, A. Merati, Y. Abu-Lebdeh, Perovskite Solid-State electrolytes for lithium metal batteries, Batteries 7 (4) (2021) 75, https://doi.org/10.3390/BATTERIES7040075.
[16] V. Veerapandiyan, F. Benes, T. Gindel, M. Deluca, Strategies to improve the energy storage properties of perovskite Lead-Free relaxor ferroelectrics: a review, Materials 13 (2020) 1–47, https://doi.org/10.3390/ma13245742.
[17] L. Shu, J. Sunarso, S.S. Hashim, J. Mao, W. Zhou, F. Liang, Advanced perovskite anodes for solid oxide fuel cells: a review, Int. J. Hydrog. Energy 44 (59) (2019) 31275–31304, https://doi.org/10.1016/J.IJHYDENE.2019.09.220.
[18] L. Paramanik, S. Subudhi, K.M. Parida, Visible light active titanate perovskites: an overview on its synthesis, characterization and photocatalytic applications, Mater. Res. Bull. 155 (2022) 111965, https://doi.org/10.1016/J.MATERRESBULL.2022.111965.
[19] D.D. Athayde, D.F. Souza, A.M.A. Silva, D. Vasconcelos, E.H.M. Nunes, J.C. Diniz, W.L. Vasconcelos, Review of perovskite ceramic synthesis and membrane

preparation methods, Ceram. Int. 42 (6) (2016) 6555–6571, https://doi.org/10.1016/j.ceramint.2016.01.130.
[20] M. Biesuz, S. Grasso, V.M. Sglavo, What's new in ceramics sintering? A short report on the latest trends and future prospects, Curr. Opin. Solid State Mater. Sci. 24 (5) (2020) 100868, https://doi.org/10.1016/J.COSSMS.2020.100868.
[21] M. Heidari, A. Zamaniyan, A. SafeKordi, E. Ganji Babakhani, M. Amanipour, Effect of sintering temperature on microstructure and hydrogen permeation properties of perovskite membrane, J. Mater. Sci. Technol. 29 (2) (2013) 137–141, https://doi.org/10.1016/j.jmst.2012.12.003.
[22] J. Hötzer, M. Seiz, M. Kellner, W. Rheinheimer, B. Nestler, Phase-Field simulation of solid state sintering, Acta Mater. 164 (2019) 184–195, https://doi.org/10.1016/J.ACTAMAT.2018.10.021.
[23] X. Kuang, G. Carotenuto, L. Nicolais, A review of ceramic sintering and suggestions on reducing sintering temperatures, Adv. Perform. Mater. 4 (3) (1997) 257–274, https://doi.org/10.1023/A:1008621020555.
[24] E. Salernitano, S. Grilli, F. Mazzanti, P. Fabbri, G. Magnani, Definition of the parameters for the densification of ceramics by Two-Step solid state sintering, Open Ceram. 9 (2022) 100242, https://doi.org/10.1016/J.OCERAM.2022.100242.
[25] D. Salamon, Flash sintering and other rapid sintering techniques, Encycl. Mater. Tech. Ceram. Glass 1–3 (2021) 286–293, https://doi.org/10.1016/B978-0-12-803581-8.12116-2.
[26] R.M. German, P. Suri, S.J. Park, Review: liquid phase sintering, J. Mater. Sci. 44 (1) (2009) 1–39, https://doi.org/10.1007/S10853-008-3008-0/FIGURES/33.
[27] J.G. Pereira da Silva, M. Bram, A.M. Laptev, J. Gonzalez-Julian, Q. Ma, F. Tietz, O. Guillon, Sintering of a Sodium-Based NASICON electrolyte: a comparative study between cold, field assisted and conventional sintering methods, J. Eur. Ceram. Soc. 39 (8) (2019) 2697–2702, https://doi.org/10.1016/J.JEURCERAMSOC.2019.03.023.
[28] F.J.A. Loureiro, N. Nasani, G.S. Reddy, N.R. Munirathnam, D.P. Fagg, A review on sintering technology of proton conducting BaCeO3-BaZrO3 perovskite oxide materials for protonic ceramic fuel cells, J. Power Sources 438 (2019) 226991, https://doi.org/10.1016/J.JPOWSOUR.2019.226991.
[29] O. Guillon, J. Gonzalez-Julian, B. Dargatz, T. Kessel, G. Schierning, J. Räthel, M. Herrmann, Field-Assisted sintering Technology/Spark plasma sintering: mechanisms, materials, and technology developments, Adv. Eng. Mater. 16 (7) (2014) 830–849, https://doi.org/10.1002/ADEM.201300409.
[30] S.V. Besegatto, C.E.M. Campos, A. da Silva, S.M.A. Guelli Ulson de Souza, A. A. Ulson de Souza, S.Y. Gómez, Perovskite-Based Ca-Ni-Fe oxides for azo pollutants fast abatement through dark catalysis, Appl. Catal. B Environ. (2020) *284*, https://doi.org/10.1016/j.apcatb.2020.119747.
[31] S. Supriya, Tailoring layered structure of Bismuth-Based aurivillius perovskites: recent advances and future aspects, Coord. Chem. Rev. 479 (2023) 215010, https://doi.org/10.1016/J.CCR.2022.215010.
[32] W.J. Yin, B. Weng, J. Ge, Q. Sun, Z. Li, Y. Yan, Oxide perovskites, double perovskites and derivatives for electrocatalysis, photocatalysis, and photovoltaics, Energy Environ. Sci. 12 (2) (2019) 442–462, https://doi.org/10.1039/c8ee01574k.
[33] J. Kong, T. Yang, Z. Rui, H. Ji, Perovskite-Based photocatalysts for organic contaminants removal: current status and future perspectives, Catal. Today 327 (2019) 47–63, https://doi.org/10.1016/j.cattod.2018.06.045.
[34] P. Kanhere, Z. Chen, A review on visible light active Perovskite-Based photocatalysts, Molecules 19 (2014) 19995–20022, https://doi.org/10.3390/molecules191219995.
[35] M. Johnsson, P. Lemmens, Perovskites and thin Films—Crystallography and chemistry, J. Phys. Condens. Matter 20 (26) (2008) 264001, https://doi.org/10.1088/0953-8984/20/26/264001.
[36] Y. Iriani, D.K. Sandi, Kusumandari, N. Sarifah, Investigation of barium strontium titanate (Ba0.95Sr0.05TiO3) synthesized via conventional Solid-State reaction and Co-Precipitation route with diverse sintering temperatures, Mater. Today. Proc. (2023), https://doi.org/10.1016/J.MATPR.2023.02.229.
[37] M. Bacha, A. Saadoune, I. Youcef, O. Terghini, Design and numerical investigation of Perovskite/Silicon tandem solar cell, Opt. Mater. 131 (2022) 112671, https://doi.org/10.1016/J.OPTMAT.2022.112671.
[38] Y. Hu, L. Mao, X. Guan, K.A. Tucker, H. Xie, X. Wu, J. Shi, Layered perovskite oxides and their derivative nanosheets adopting different modification strategies towards better photocatalytic performance of water splitting, Renew. Sustain. Energy Rev. 119 (2020) 109527, https://doi.org/10.1016/J.RSER.2019.109527.
[39] Y. Zhou, Y. Zhao, Chemical stability and instability of inorganic halide perovskites, Energy Environ. Sci. 12 (5) (2019) 1495–1511, https://doi.org/10.1039/c8ee03559h.
[40] G. Zhang, G. Liu, L. Wang, J.T.S. Irvine, Inorganic perovskite photocatalysts for solar energy utilization, Chem. Soc. Rev. 45 (2016) 5951–5984, https://doi.org/10.1039/c5cs00769k.
[41] T. Liu, N.P. Holzapfel, P.M. Woodward, Understanding structural distortions in hybrid layered perovskites with the $n = 1$ Ruddlesden-Popper structure, IUCrJ 10 (2023) 385–396, https://doi.org/10.1107/S2052252523003743.
[42] A.N. Zainon, M.R. Somalu, A.M.K. Bahrain, A. Muchtar, N.A. Baharuddin, M. A. Muhammed, A. Abdul Samat, N. Osman, A.K. Azad, Influence of sintering temperature on the properties of the Screen-Printed anode of the LSMO4 Ruddlesden-Popper perovskite for Intermediate-Temperature solid oxide fuel cells, Int. J. Hydrog. Energy (2023), https://doi.org/10.1016/J.IJHYDENE.2023.06.139.
[43] J.M. Bassat, P. Odier, A. Villesuzanne, C. Marin, M. Pouchard, Anisotropic ionic transport properties in La2NiO 4+δ single crystals, Solid State Ion. 167 (3–4) (2004) 341–347, https://doi.org/10.1016/j.ssi.2003.12.012.
[44] P. Ding, W. Li, H. Zhao, C. Wu, L. Zhao, B. Dong, S. Wang, Review on Ruddlesden-Popper perovskites as cathode for solid oxide fuel cells, JPhys Mater. 4 (2) (2021), https://doi.org/10.1088/2515-7639/abe392.
[45] R. Pelosato, G. Cordaro, D. Stucchi, C. Cristiani, G. Dotelli, Cobalt based layered perovskites as cathode material for intermediate temperature solid oxide fuel cells: a brief review, J. Power Sources 298 (2015) 46–67, https://doi.org/10.1016/J.JPOWSOUR.2015.08.034.
[46] M.D. Smith, B.A. Connor, H.I. Karunadasa, Tuning the luminescence of layered halide perovskites, Chem. Rev. 119 (5) (2019) 3104–3139, https://doi.org/10.1021/acs.chemrev.8b00477.
[47] H. Chen, M. Li, B. Wang, S. Ming, J. Su, Structure, electronic and optical properties of CsPbX3 halide perovskite: a First-Principles study, J. Alloy. Compd. 862 (2021) 158442, https://doi.org/10.1016/J.JALLCOM.2020.158442.
[48] T.H. Bui, J.H. Shin, Perovskite materials for sensing applications: recent advances and challenges, Microchem. J. 191 (2023) 108924, https://doi.org/10.1016/J.MICROC.2023.108924.
[49] A. Hossain, P. Bandyopadhyay, A. Karmakar, A.K.M.A. Ullah, R.K. Manavalan, K. Sakthipandi, N. Alhokbany, S.M. Alshehri, J. Ahmed, The hybrid halide perovskite: synthesis strategies, fabrications, and modern applications, Ceram. Int. 48 (6) (2022) 7325–7343, https://doi.org/10.1016/j.ceramint.2021.11.313.
[50] A. Mathur, H. Fan, V. Maheshwari, Organolead halide perovskites beyond solar cells: Self-Powered devices and the associated progress and challenges, Mater. Adv. 2 (2021) 5274–5299, https://doi.org/10.1039/d1ma00377a.
[51] N.J. Jeon, J.H. Noh, W.S. Yang, Y.C. Kim, S. Ryu, J. Seo, S.I. Seok, Compositional engineering of perovskite materials for High-Performance solar cells, Nature 517 (7535) (2015) 476–480, https://doi.org/10.1038/NATURE14133.
[52] K. Nishi, T. Oku, T. Kishimoto, N. Ueoka, A. Suzuki, Photovoltaic characteristics of CH3NH3PbI3 perovskite solar cells added with ethylammonium bromide and formamidinium iodide, Coatings 10 (4) (2020), https://doi.org/10.3390/coatings10040410.
[53] C.A. Orge, J.J.M. Órfão, M.F.R. Pereira, B.P. Barbero, L.E. Cadús, Lanthanum-Based perovskites as catalysts for the ozonation of selected organic compounds, Appl. Catal. B Environ. 140–141 (2013) 426–432, https://doi.org/10.1016/j.apcatb.2013.04.045.
[54] B.J. Martynczuk, M. Arnold, H. Wang, J. Caro, A. Feldhoff, Perovskites form via an EDTA/ citric acid complexing method, Adv. Mater. 510640 (2007) 2134–2140, https://doi.org/10.1002/adma.200700322.
[55] G. Sachinelli, P. Lemes, R. Antonio, F. Machado, D. Hotza, Membranas de Condução mista Iônica e Eletrônica (MIEC): Composições, Preparação e desempenho, Quim. Nova 37 (2) (2014) 302–307, https://doi.org/10.5935/0100-4042.20140051.
[56] T. Velempini, E. Prabakaran, K. Pillay, Recent developments in the use of metal oxides for photocatalytic degradation of pharmaceutical pollutants in Water—a review, Mater. Today Chem. 19 (2021) 100380, https://doi.org/10.1016/j.mtchem.2020.100380.
[57] A. Feldhoff, M. Arnold, J. Martynczuk, T.M. Gesing, H. Wang, The Sol-Gel synthesis of perovskites by an EDTA/Citrate complexing method involves nanoscale solid state reactions, Solid State Sci. 10 (6) (2008) 689–701, https://doi.org/10.1016/j.solidstatesciences.2007.11.030.
[58] G. Jayanthi, S. Sumathi, K. Kannan, V. Andal, S. Murugan, A review on synthesis, properties, and environmental application of Fe-Based perovskite, Adv. Mater. Sci. Eng. 2022 (2022), https://doi.org/10.1155/2022/6607683.
[59] V. Vendruscolo, D.L. Fritzen, E.A. de Mattos, L.C.V. Rodrigues, 15 - light storage perovskites: synthesis, mechanisms, and applications, in: J.L.C. Huamán, V.A. G. Rivera (Eds.), In Perovskite Ceramics, Elsevier, 2023, pp. 517–546, https://doi.org/10.1016/B978-0-323-90586-2.00013-9.
[60] M. Humayun, F. Raziq, A. Khan, W. Luo, Modification strategies of TiO_2 for potential applications in photocatalysis: a critical review, Green. Chem. Lett. Rev. 11 (2) (2018) 86–102, https://doi.org/10.1080/17518253.2018.1440324.
[61] R.E.A. Ngida, M.F. Zawrah, R.M. Khattab, E. Heikal, Hydrothermal synthesis, sintering and characterization of nano La-Manganite perovskite doped with ca or sr, Ceram. Int. 45 (4) (2019) 4894–4901, https://doi.org/10.1016/j.ceramint.2018.11.188.
[62] R.I. Walton, Perovskite oxides prepared by hydrothermal and solvothermal synthesis: a review of crystallisation, chemistry, and compositions, Chem. A Eur. J. 26 (42) (2020) 9041–9069, https://doi.org/10.1002/chem.202000707.
[63] K. ichi Mimura, N. Hamao, H. Itasaka, Z. Liu, K. Hamamoto, Hydrothermal synthesis of Perovskite-Type solid electrolyte nanoplate, J. Sol. Gel Sci. Technol. 104 (3) (2022) 599–605, https://doi.org/10.1007/s10971-022-05810-3.
[64] T.R.N. Kutty, R. Vivekanandan, Preparation of CaTiO3 fine powders by the hydrothermal method, Mater. Lett. 5 (3) (1987) 79–83.
[65] K.O. Ogunniran, G. Murugadoss, R. Thangamuthu, P. Periasamy, Evaluation of nanostructured Nd0.7Co0.3FeO3 perovskite obtained via hydrothermal method as anode material for Li-Ion battery, Mater. Chem. Phys. 248 (February) (2020) 122944, https://doi.org/10.1016/j.matchemphys.2020.122944.
[66] J.C. Rendón-Angeles, K. Yanagisawa, Z. Matamoros-Veloza, M.I. Pech-Canul, J. Mendez-Nonell, S.D.D.L. Torre, Hydrothermal synthesis of perovskite strontium doped lanthanum chromite fine powders and its sintering, J. Alloy. Compd. 504 (1) (2010) 251–256, https://doi.org/10.1016/j.jallcom.2010.05.103.
[67] H. Ou, M. Sahli, J.C. Gelin, T. Barrière, Experimental analysis and finite element simulation of the Co-Sintering of Bi-Material components, Powder Technol. 268 (2014) 269–278, https://doi.org/10.1016/j.powtec.2014.08.023.
[68] B. Ratzker, M. Sokol, Exploring the capabilities of High-Pressure spark plasma sintering (HPSPS): a review of materials processing and properties, Mater. Des. 233 (April) (2023) 112238, https://doi.org/10.1016/j.matdes.2023.112238.

[69] P. Dahl, I. Kaus, Z. Zhao, M. Johnsson, M. Nygren, K. Wiik, T. Grande, M. A. Einarsrud, Densification and properties of zirconia prepared by three different sintering techniques, Ceram. Int. 33 (8) (2007) 1603–1610, https://doi.org/10.1016/J.CERAMINT.2006.07.005.
[70] M.R. Mazlan, N.H. Jamadon, A. Rajabi, A.B. Sulong, I.F. Mohamed, F. Yusof, N. A. Jamal, Necking mechanism under various sintering process parameters – a review, J. Mater. Res. Technol. 23 (2023) 2189–2201, https://doi.org/10.1016/j.jmrt.2023.01.013.
[71] R. de Oro Calderon, C. Gierl-Mayer, H. Danninger, Fundamentals of sintering: liquid phase sintering. In Encyclopedia of Materials: Metals and Alloys, Elsevier, 2022, pp. 481–492, https://doi.org/10.1016/B978-0-12-819726-4.00127-7.
[72] A. Pakdel, A. Witecka, G. Rydzek, D.N. Awang Shri, A comprehensive microstructural analysis of Al–WC Micro- and Nano-Composites prepared by spark plasma sintering, Mater. Des. 119 (2017) 225–234, https://doi.org/10.1016/j.matdes.2017.01.064.
[73] A. Ishii, K. Kondo, A. Yamamoto, A. Yamanaka, Phase-Field modeling of Solid-State sintering with interfacial anisotropy, Mater. Today Commun. 35 (2023) 106061, https://doi.org/10.1016/J.MTCOMM.2023.106061.
[74] Q. Yang, Y. Gao, A. Kirshtein, Q. Zhen, C. Liu, A Free-Energy-Based and interfacially consistent Phase-Field model for Solid-State sintering without artificial void generation, Comput. Mater. Sci. 229 (2023) 112387, https://doi.org/10.1016/J.COMMATSCI.2023.112387.
[75] Y. Ni, K. Liu, J. Wang, H. Sun, Y. Du, W. Liu, Establishment of constitutive models and numerical simulation of dry pressing and solid state sintering processes of MgTiO3 ceramic, Ceram. Int. 47 (7) (2021) 8769–8780, https://doi.org/10.1016/J.CERAMINT.2020.11.242.
[76] D. Han, Y. Otani, Y. Noda, T. Onishi, M. Majima, T. Uda, Strategy to improve phase compatibility between proton conductive BaZr0.8Y0.2O3−δ and nickel oxide, RSC Adv. 6 (23) (2016) 19288–19297, https://doi.org/10.1039/C5RA26947D.
[77] M. Shirpour, B. Rahmati, W. Sigle, P.A. Van Aken, R. Merkle, J. Maier, Dopant segregation and space charge effects in Proton-Conducting BaZrO 3 perovskites, J. Phys. Chem. C. 116 (2012) 2453–2461, https://doi.org/10.1021/jp208213x.
[78] J.W. Stevenson, T.R. Armstrong, L.R. Pederson, J. Li, C.A. Lewinsohn, S. Baskaran, Effect of A-Site cation nonstoichiometry on the properties of doped lanthanum gallate, Solid State Ion. 113–115 (1998) 571–583, https://doi.org/10.1016/S0167-2738(98)00324-5.
[79] J.G. Pereira da Silva, M. Bram, A.M. Laptev, J. Gonzalez-Julian, Q. Ma, F. Tietz, O. Guillon, Sintering of a Sodium-Based NASICON electrolyte: a comparative study between cold, field assisted and conventional sintering methods, J. Eur. Ceram. Soc. 39 (8) (2019) 2697–2702, https://doi.org/10.1016/J.JEURCERAMSOC.2019.03.023.
[80] S.H. Huo, M. Qian, G.B. Schaffer, E. Crossin, Aluminium powder metallurgy, Fundam. Alum. Metall. Prod. Process. Appl. (2011) 655–701, https://doi.org/10.1533/9780857090256.3.655.
[81] P.S. Charan, A. Vijay, R. Jose, K. Venkata Saravanan, Liquid phase sintering of nb doped SrTiO3-δ ceramics with enhanced thermoelectric figure of merit, Ceram. Int. 49 (11) (2023) 19043–19053, https://doi.org/10.1016/J.CERAMINT.2023.03.031.
[82] T. Wei, X. Liu, C. Yuan, Q. Gao, X. Xin, S. Wang, A modified Liquid-Phase-Assisted sintering mechanism for La0.8Sr0.2Cr1−xFexO3−δ—A high density, Redox-Stable perovskite interconnect for solid oxide fuel cells, J. Power Sources 250 (2014) 152–159, https://doi.org/10.1016/j.jpowsour.2013.11.012.
[83] S. Cohen, B. Ratzker, S. Kalabukhov, N. Frage, Diffusion bonding of transparent ceramics by spark plasma sintering (SPS) complemented by hot isostatic pressing (HIP), J. Eur. Ceram. Soc. 43 (14) (2023) 6628–6633, https://doi.org/10.1016/j.jeurceramsoc.2023.06.071.
[84] A. Mei, Q.H. Jiang, Y.H. Lin, C.W. Nan, Lithium lanthanum titanium oxide Solid-State electrolyte by spark plasma sintering, J. Alloy. Compd. 486 (1–2) (2009) 871–875, https://doi.org/10.1016/j.jallcom.2009.07.091.
[85] Y.X. Gao, X.P. Wang, Q.X. Sun, Z. Zhuang, Q.F. Fang, Electrical properties of Garnet-like lithium ionic conductors li 5+xSr xla 3-xBi 2O 12 fabricated by spark plasma sintering method, Front. Mater. Sci. 6 (3) (2012) 216–224, https://doi.org/10.1007/s11706-012-0172-6.
[86] F. Delorme, C. Chen, F. Schoenstein, N. Jaber, F. Jean, M. Bah, Q. Simon, T. Chartier, P. Laffez, I. Monot-Laffez, F. Giovannelli, Low intrinsic thermal conductivity of spark plasma sintered dense KNbO3 and NaNbO3 perovskite ceramics, Thermochim. Acta 695 (August 2020) (2021) 178807, https://doi.org/10.1016/j.tca.2020.178807.
[87] S.N. Sari, P. Nieroda, P. Pasierb, The BaCeO3-Based composite protonic conductors prepared by spark plasma sintering (SPS) and Free-Sintering methods, Int. J. Hydrog. Energy 48 (76) (2023) 29748–29758, https://doi.org/10.1016/j.ijhydene.2023.04.138.
[88] S. Ricote, N. Bonanos, H.J. Wang, B.A. Boukamp, Conductivity study of dense BaZr0.9Y0.1O(3 − δ) obtained by spark plasma sintering, Solid State Ion. 213 (2012) 36–41, https://doi.org/10.1016/J.SSI.2011.02.011.
[89] A. Rečnik, D. Kolar, Exaggerated growth of hexagonal barium titanate under reducing sintering conditions, J. Am. Ceram. Soc. 79 (4) (1996) 1015–1018, https://doi.org/10.1111/J.1151-2916.1996.TB08541.X.
[90] H.M. Kotb, M.M. Ahmad, S. Aldabal, A. Alshoaibi, A. Aljaafari, Structural and dielectric behavior of Al-Substituted CaCu3Ti4O12 ceramics with giant dielectric constant by spark plasma sintering, Journal Materials Science Materials Electronics 30 (19) (2019) 18259–18267, https://doi.org/10.1007/S10854-019-02180-5/FIGURES/12.
[91] L. Cheng, S. Jiang, Q. Ma, Z. Shang, S. Liu, Sintering behavior and microwave properties of dense 0.7CaTiO3-0.3NdAlO3 ceramics with Sub-Micron sized grains by spark plasma sintering, Scr. Mater. 115 (2016) 80–83, https://doi.org/10.1016/j.scriptamat.2016.01.003.
[92] S.H. Song, Q.S. Zhu, L.Q. Weng, V.R. Mudinepalli, A comparative study of dielectric, ferroelectric and magnetic properties of BiFeO3 multiferroic ceramics synthesized by conventional and spark plasma sintering techniques, J. Eur. Ceram. Soc. 35 (1) (2015) 131–138, https://doi.org/10.1016/J.JEURCERAMSOC.2014.08.016.
[93] J. Hong, L. Gao, S.D.D.L. Torre, H. Miyamoto, K. Miyamoto, Spark plasma sintering and mechanical properties of ZrO2(Y2O3)–Al2O3 composites, Mater. Lett. 43 (1–2) (2000) 27–31, https://doi.org/10.1016/S0167-577X(99)00225-6.
[94] T.L. Simonenko, M.V. Kalinina, N.P. Simonenko, E.P. Simonenko, O.V. Glumov, N.A. Mel'nikova, I.V. Murin, O.O. Shichalin, E.K. Papynov, O.A. Shilova, V. G. Sevastyanov, N.T. Kuznetsov, Synthesis of BaCe0.9-xZrxY0.1O3-δ nanopowders and the study of proton conductors fabricated on their basis by Low-Temperature spark plasma sintering, Int. J. Hydrog. Energy 44 (36) (2019) 20345–20354, https://doi.org/10.1016/J.IJHYDENE.2019.05.231.
[95] C. Manière, G. Riquet, S. Marinel, Dielectric properties of flash spark plasma sintered BaTiO3 and CaCu3Ti4O12, Scr. Mater. 173 (2019) 41–45, https://doi.org/10.1016/J.SCRIPTAMAT.2019.07.048.
[96] R. Yu, Q.X. Du, B.K. Zou, Z.Y. Wen, C.H. Chen, Synthesis and characterization of Perovskite-Type (Li,Sr)(Zr,Nb)O3 quaternary solid electrolyte for All-Solid-State batteries, J. Power Sources 306 (2016) 623–629, https://doi.org/10.1016/J.JPOWSOUR.2015.12.065.
[97] G. Li, Y. Wang, L. Huang, W. Sun, Research progress of High-Sensitivity perovskite photodetectors: a review of photodetectors: noise, structure, and materials, ACS Appl. Electron. Mater. 4 (4) (2022) 1485–1505, https://doi.org/10.1021/ACSAELM.1C01349/ASSET/IMAGES/LARGE/EL1C01349_0009.JPEG.
[98] J.Y. Kim, J.W. Lee, H.S. Jung, H. Shin, N.G. Park, High-Efficiency perovskite solar cells, Chem. Rev. 120 (15) (2020) 7867–7918, https://doi.org/10.1021/ACS.CHEMREV.0C00107/ASSET/IMAGES/MEDIUM/CR0C00107_M019.GIF.
[99] J. Lu, Y. Li, Perovskite-type Li-ion solid electrolytes: a review, Journal Materials Science Materials Electronics 32 (8) (2021) 9736–9754, https://doi.org/10.1007/S10854-021-05699-8.
[100] M. Ahangari, J. Mostafaei, A. Sayyah, E. Mahmoudi, E. Asghari, A. Coruh, N. Delibas, A. Niaei, Investigation of structural and electrochemical properties of SrFexCo1-xO3-δ perovskite oxides as a supercapacitor electrode material, J. Energy Storage 63 (2023) 107034, https://doi.org/10.1016/J.EST.2023.107034.
[101] F. Li, J. Zhai, B. Shen, H. Zeng, Recent progress of ecofriendly Perovskite-Type dielectric ceramics for energy storage applications, J. Adv. Dielectr. 8 (6) (2018), https://doi.org/10.1142/S2010135X18300050.
[102] P.J. Hall, E.J. Bain, Energy-Storage technologies and electricity generation, Energy Policy 36 (12) (2008) 4352–4355, https://doi.org/10.1016/J.ENPOL.2008.09.037.
[103] H. Palneedi, M. Peddigari, G.T. Hwang, D.Y. Jeong, J. Ryu, High-Performance dielectric ceramic films for energy storage capacitors: progress and outlook, Adv. Funct. Mater. 28 (42) (2018) 1803665, https://doi.org/10.1002/ADFM.201803665.
[104] P.C. Himadri Reddy, J. Amalraj, S. Ranganatha, S.S. Patil, S. Chandrasekaran, A review on effect of conducting polymers on Carbon-Based electrode materials for electrochemical supercapacitors, Synth. Met. 298 (2023) 117447, https://doi.org/10.1016/J.SYNTHMET.2023.117447.
[105] R. Das, R.N.P. Choudhary, Structural and electrical properties of double perovskite: (BaSr)FeMoO6, Physica B Condensed Matter 603 (2021) 412522, https://doi.org/10.1016/J.PHYSB.2020.412522.
[106] L. Sahoo, B.N. Parida, R.K. Parida, R. Padhee, A.K. Mahapatra, Structural, optical dielectric and ferroelectric properties of double perovskite BaBiFeTiO6, Inorg. Chem. Commun. 146 (2022) 110102, https://doi.org/10.1016/J.INOCHE.2022.110102.
[107] Y. Liu, T. He, J. Zeng, Dielectric property of perovskite La0.86Cu3Ti3.42Al0.58O12 ceramic, Ferroelectrics 568 (1) (2020) 123–131, https://doi.org/10.1080/00150193.2020.1811036.
[108] A.K. Yadav, C. Gautam, Dielectric behavior of perovskite glass ceramics, Journal Materials Science Materials Electronics 25 (12) (2014) 5165–5187, https://doi.org/10.1007/S10854-014-2311-6/TABLES/1.
[109] K.Y. Chan, B. Jia, H. Lin, N. Hameed, J.H. Lee, K.T. Lau, A critical review on multifunctional composites as structural capacitors for energy storage, Compos. Struct. 188 (2018) 126–142, https://doi.org/10.1016/J.COMPSTRUCT.2017.12.072.
[110] G. Li, Y. Zhang, L. Wu, F. Wu, R. Wang, D. Zhang, J. Zhu, H. Li, An efficient Round-the-Clock la 2 NiO 4 catalyst for breaking down phenolic pollutants, RSC Adv. 2 (11) (2012) 4822–4828, https://doi.org/10.1039/C2RA20233F.
[111] B.A. Bender, M.J. Pan, The effect of processing on the giant dielectric properties of CaCu3Ti4O12, Materials Science Engineering B 117 (3) (2005) 339–347, https://doi.org/10.1016/J.MSEB.2004.11.019.
[112] K. Singh, S.A. Band, W.K. Kinge, Effect of sintering temperature on dielectric properties of Pb(Fe1/2Nb1/2)O3 perovskite material, Ferroelectrics 306 (1) (2004) 179–185, https://doi.org/10.1080/00150190490460821.
[113] S. Pandey, V. Kumar, K.D. Mandal, Studies of sintering temperature on the microstructure, magnetic and dielectric behavior of CaCu3Ti3.5Mn0.5O12 ceramic synthesized by Semi-Wet route, SN Appl. Sci. 2 (3) (2020) 1–9, https://doi.org/10.1007/S42452-020-2282-6/FIGURES/10.
[114] L. Chun Yan, J. Hassan, M. Hashim, W. Swee Yin, T. Foo Khoon, W. Yick Jeng, Effect of sintering temperatures on the microstructure and dielectric properties of SrTiO 3, World Appl. Sci. J. 15 (11) (2011) 1614–1618.

[115] J. Shanker, Influence of sintering temperature on electrical properties of fe substituted NdCrO3 relaxor perovskite ceramic materials, Materials Science Engineering B 286 (2022) 116039, https://doi.org/10.1016/J.MSEB.2022.116039.
[116] T.M. Abd Allah, A. Elfalaky, M.H. Ghozza, Effect of sintering on formation, structure, magnetic and dielectric properties of nanocrystalline La0.1Ca0.9MnO3 perovskite, Materials Science Engineering B 281 (2022) 115749, https://doi.org/10.1016/J.MSEB.2022.115749.
[117] A.R. Jayakrishnan, J.P.B. Silva, K. Kamakshi, D. Dastan, V. Annapureddy, M. Pereira, K.C. Sekhar, Are Lead-Free relaxor ferroelectric materials the most promising candidates for energy storage capacitors? Prog. Mater. Sci. 132 (2023) 101046 https://doi.org/10.1016/J.PMATSCI.2022.101046.
[118] J. Yin, Y. Zhang, X. Lv, J. Wu, Ultrahigh Energy-Storage potential under low electric field in bismuth sodium Titanate-Based perovskite ferroelectrics, J. Mater. Chem. A 6 (21) (2018) 9823–9832, https://doi.org/10.1039/C8TA00474A.
[119] A. Mishra, B. Majumdar, R. Ranjan, A complex Lead-Free (Na, Bi, Ba)(Ti, Fe)O3 single phase perovskite ceramic with a high Energy-Density and high Discharge-Efficiency for solid state capacitor applications, J. Eur. Ceram. Soc. 37 (6) (2017) 2379–2384, https://doi.org/10.1016/J.JEURCERAMSOC.2017.01.036.
[120] H.Y. Zhou, X.Q. Liu, X.L. Zhu, X.M. Chen, CaTiO3 linear dielectric ceramics with greatly enhanced dielectric strength and energy storage density, J. Am. Ceram. Soc. 101 (5) (2018) 1999–2008, https://doi.org/10.1111/JACE.15371.
[121] Y.J. Wu, Y.H. Huang, N. Wang, J. Li, M.S. Fu, X.M. Chen, Effects of phase constitution and microstructure on energy storage properties of barium strontium titanate ceramics, J. Eur. Ceram. Soc. 37 (5) (2017) 2099–2104, https://doi.org/10.1016/J.JEURCERAMSOC.2016.12.052.
[122] P. Ren, Q. Wang, S. Li, G. Zhao, Energy storage density and tunable dielectric properties of BaTi0.85Sn0.15O3/MgO composite ceramics prepared by SPS, J. Eur. Ceram. Soc. 37 (4) (2017) 1501–1507, https://doi.org/10.1016/J.JEURCERAMSOC.2016.12.016.
[123] Y.H. Huang, Y.J. Wu, W.J. Qiu, J. Li, X.M. Chen, Enhanced energy storage density of Ba0.4Sr0.6TiO3–MgO composite prepared by spark plasma sintering, J. Eur. Ceram. Soc. 35 (5) (2015) 1469–1476, https://doi.org/10.1016/j.jeurceramsoc.2014.11.022.
[124] B. Qu, H. Du, Z. Yang, Q. Liu, Large recoverable energy storage density and low sintering temperature in Potassium-Sodium Niobate-Based ceramics for multilayer pulsed power capacitors, J. Am. Ceram. Soc. 100 (4) (2017) 1517–1526, https://doi.org/10.1111/JACE.14728.
[125] B. Qu, H. Du, Z. Yang, Q. Liu, T. Liu, Enhanced dielectric breakdown strength and energy storage density in Lead-Free relaxor ferroelectric ceramics prepared using transition liquid phase sintering, RSC Adv. 6 (41) (2016) 34381–34389, https://doi.org/10.1039/c6ra01919f.
[126] L. Zhang, X. Pu, M. Chen, S. Bai, Y. Pu, Influence of BaSnO3 additive on the energy storage properties of Na0.5Bi0.5TiO3-Based relaxor ferroelectrics, J. Eur. Ceram. Soc. 38 (5) (2018) 2304–2311, https://doi.org/10.1016/J.JEURCERAMSOC.2017.11.053.
[127] J. Wu, A. Mahajan, L. Riekehr, H. Zhang, B. Yang, N. Meng, Z. Zhang, H. Yan, Perovskite Srx(Bi1−xNa0.97−xLi0.03)0.5TiO3 ceramics with polar nano regions for high power energy storage, Nano Energy 50 (2018) 723–732, https://doi.org/10.1016/J.NANOEN.2018.06.016.
[128] A.K. Yadav, H. Fan, B. Yan, C. Wang, M. Zhang, J. Ma, W. Wang, W. Dong, S. Wang, High energy storage density and stable fatigue resistance of Na0.46Bi0.46Ba0.05La0.02Zr0.03Ti0.97-xSnxO3 ceramics, Ceram. Int. 46 (5) (2020) 5681–5688, https://doi.org/10.1016/J.CERAMINT.2019.11.015.
[129] X. Qiao, D. Wu, F. Zhang, M. Niu, B. Chen, X. Zhao, P. Liang, L. Wei, X. Chao, Z. Yang, Enhanced energy density and thermal stability in relaxor ferroelectric Bi0.5Na0.5TiO3-Sr0.7Bi0.2TiO3 ceramics, J. Eur. Ceram. Soc. 39 (15) (2019) 4778–4784, https://doi.org/10.1016/J.JEURCERAMSOC.2019.07.003.
[130] Z. Jiang, Y. Yuan, H. Yang, E. Li, S. Zhang, Excellent thermal stability and energy storage properties of Lead-Free Bi0.5Na0.5TiO3-Based ceramic, J. Am. Ceram. Soc. 105 (6) (2022) 4027–4038, https://doi.org/10.1111/JACE.18332.
[131] Y. Xu, Z. Yang, K. Xu, J. Tian, D. Zhang, M. Zhan, H. Tian, X. Cai, B. Zhang, Y. Yan, L. Guo, G. Wang, L. Lin, J. Fan, T. Wang, Y. Tian, Enhanced Energy-Storage performance in silver Niobate-Based dielectric ceramics sintered at low temperature, J. Alloy. Compd. 913 (2022) 165313, https://doi.org/10.1016/J.JALLCOM.2022.165313.
[132] W. Wang, Y. Pu, X. Guo, R. Shi, M. Yang, J. Li, Enhanced energy storage and fast Charge-Discharge capability in Ca0.5Sr0.5TiO3-Based linear dielectric ceramic, J. Alloy. Compd. 817 (2020) 152695, https://doi.org/10.1016/J.JALLCOM.2019.152695.
[133] Z. Yao, Q. Luo, G. Zhang, H. Hao, M. Cao, H. Liu, Improved Energy-Storage performance and breakdown enhancement mechanism of Mg-Doped SrTiO3 bulk ceramics for high energy density capacitor applications, Journal Materials Science Materials Electronics 28 (15) (2017) 11491–11499, https://doi.org/10.1007/S10854-017-6945-Z/FIGURES/6.
[134] C. Xu, X. Zhao, L. Ren, J. Sun, L. Yang, J. Guo, R. Liao, Enhanced electrical properties of CaCu3Ti4O12 ceramics by spark plasma sintering: role of zn and al Co-Doping, J. Alloy. Compd. 792 (2019) 1079–1087, https://doi.org/10.1016/J.JALLCOM.2019.04.131.
[135] Y. Lu, H. Zhang, H. Yang, P. Fan, C. Samart, N. Takesue, H. Tan, SPS-Prepared High-Entropy (Bi0.2Na0.2Sr0.2Ba0.2Ca0.2)TiO3 Lead-Free Relaxor-Ferroelectric ceramics with high energy storage density, Crystals 13 (3) (2023) 445, https://doi.org/10.3390/CRYST13030445/S1.
[136] L. Yang, X. Kong, F. Li, H. Hao, Z. Cheng, H. Liu, J.F. Li, S. Zhang, Perovskite Lead-Free dielectrics for energy storage applications, Prog. Mater. Sci. 102 (2019) 72–108, https://doi.org/10.1016/J.PMATSCI.2018.12.005.
[137] Z. Peng, J. Wang, P. Liang, J. Zhu, X. Zhou, X. Chao, Z. Yang, A new Perovskite-Related ceramic with colossal permittivity and low dielectric loss, J. Eur. Ceram. Soc. 40 (12) (2020) 4010–4015, https://doi.org/10.1016/J.JEURCERAMSOC.2020.04.030.
[138] B. Gupta, M.A. Hossain, A. Riaz, A. Sharma, D. Zhang, H.H. Tan, C. Jagadish, K. Catchpole, B. Hoex, S. Karuturi, Recent advances in materials design using atomic layer deposition for energy applications, Adv. Funct. Mater. 32 (3) (2022), https://doi.org/10.1002/ADFM.202109105.
[139] H. Mo, H. Nan, X. Lang, S. Liu, L. Qiao, X. Hu, H. Tian, Influence of calcium doping on performance of LaMnO3 supercapacitors, Ceram. Int. 44 (8) (2018) 9733–9741, https://doi.org/10.1016/J.CERAMINT.2018.02.205.
[140] S. Samantaray, D. Mohanty, I.M. Hung, M. Moniruzzaman, S.K. Satpathy, Unleashing recent electrolyte materials for Next-Generation supercapacitor applications: a comprehensive review, J. Energy Storage 72 (2023) 108352, https://doi.org/10.1016/J.EST.2023.108352.
[141] Poonam, K. Sharma, A. Arora, S.K. Tripathi, Review of supercapacitors: materials and devices, J. Energy Storage 21 (2019) 801–825, https://doi.org/10.1016/J.EST.2019.01.010.
[142] P. Phumuen, P. Kumnorkaew, P. Srepusharawoot, P. Klangtakai, S. Pimanpang, V. Amornkitbamrung, Ball milling modification of perovskite LaNiO3 powders for enhancing electrochemical pseudocapacitor, Surf. Interfaces 25 (2021) 101282, https://doi.org/10.1016/J.SURFIN.2021.101282.
[143] C.T. Alexander, J.T. Mefford, J. Saunders, R.P. Forslund, K.P. Johnston, K. J. Stevenson, Anion-Based pseudocapacitance of the perovskite library la 1- x sr x BO 3-δ (B = Fe, Mn, Co), ACS Appl. Mater. Interfaces 11 (5) (2019) 5084–5094, https://doi.org/10.1021/ACSAMI.8B19592/ASSET/IMAGES/LARGE/AM-2018-19592X_0006.JPEG.
[144] W. Che, M. Wei, Z. Sang, Y. Ou, Y. Liu, J. Liu, Perovskite LaNiO3-δ oxide as an Anion-Intercalated pseudocapacitor electrode, J. Alloy. Compd. 731 (2018) 381–388, https://doi.org/10.1016/J.JALLCOM.2017.10.027.
[145] L.C.C.B. Oliveira, R. Venâncio, P. V. F. de Azevedo, C.G. Anchieta, T. C. M. Nepel, C.B. Rodella, H. Zanin, G. Doubek, Reviewing perovskite oxide sites influence on electrocatalytic reactions for high energy density devices, J. Energy Chem. 81 (2023) 1–19, https://doi.org/10.1016/J.JECHEM.2023.02.013.
[146] G. George, S.L. Jackson, C.Q. Luo, D. Fang, D. Luo, D. Hu, J. Wen, Z. Luo, Effect of doping on the performance of High-Crystalline SrMnO3 perovskite nanofibers as a supercapacitor electrode, Ceram. Int. 44 (17) (2018) 21982–21992, https://doi.org/10.1016/J.CERAMINT.2018.08.313.
[147] Y. Liu, Z. Wang, J.P.M. Veder, Z. Xu, Y. Zhong, W. Zhou, M.O. Tade, S. Wang, Z. Shao, Highly defective layered double perovskite oxide for efficient energy storage via reversible pseudocapacitive Oxygen-Anion intercalation, Adv. Energy Mater. 8 (11) (2018) 1702604, https://doi.org/10.1002/AENM.201702604.
[148] S.T. Dong, X. Ye, Z. Fu, X. Jin, J. Wei, L. Wang, Y.M. Zhang, Effects of strontium substitution for la on the electrochemical performance of LaAlO3 perovskite nanotubes, J. Mater. Res. Technol. 19 (2022) 91–100, https://doi.org/10.1016/J.JMRT.2022.04.150.
[149] T. Gecil Evangeline, A.R. Annamalai, T.B. Magdaline, Modern synthesis and sintering techniques of calcium copper titanium oxide (CaCu3Ti4O12) ceramics and its current trend in prospective applications: a Mini-Review, Nanomaterials 12 (18) (2022), https://doi.org/10.3390/NANO12183181.
[150] S.R. Srither, N.R. Dhineshbabu, Synthesis and characterisation of FeTiO3 perovskite nanomaterials for electrochemical energy storage application, Micro Nano Lett. 14 (5) (2019) 475–478, https://doi.org/10.1049/MNL.2018.5646.
[151] S.B. Karki, F. Ramezanipour, Pseudocapacitive energy storage and electrocatalytic Hydrogen-Evolution activity of Defect-Ordered perovskites SrxCa3−xGaMn2O8 (x = 0 and 1), ACS Appl. Energy Mater. 3 (11) (2020) 10983–10992, https://doi.org/10.1021/ACSAEM.0C01935/ASSET/IMAGES/MEDIUM/AE0C01935_M010.GIF.
[152] U.C. Chung, C. Elissalde, S. Mornet, M. Maglione, C. Estournès, Controlling internal barrier in low loss BaTiO3 supercapacitors, Appl. Phys. Lett. 94 (7) (2009), https://doi.org/10.1063/1.3076125/165854.
[153] K.C. Divya, J. Østergaard, Battery energy storage technology for power Systems—An overview, Electr. Power Syst. Res. 79 (4) (2009) 511–520, https://doi.org/10.1016/J.EPSR.2008.09.017.
[154] V. Thangadurai, B. Chen, Solid Li- and Na-Ion electrolytes for next generation rechargeable batteries, Chem. Mater. 34 (15) (2022) 6637–6658, https://doi.org/10.1021/ACS.CHEMMATER.2C01475/ASSET/IMAGES/LARGE/CM2C01475_0017.JPEG.
[155] Y. Chen, Y. Kang, Y. Zhao, L. Wang, J. Liu, Y. Li, Z. Liang, X. He, X. Li, N. Tavajohi, B. Li, A review of Lithium-Ion battery safety concerns: the issues, strategies, and testing standards, J. Energy Chem. 59 (2021) 83–99, https://doi.org/10.1016/J.JECHEM.2020.10.017.
[156] A. Manthiram, X. Yu, S. Wang, Lithium battery chemistries enabled by Solid-State electrolytes, Nat. Rev. Mater. 2 (4) (2017) 1–16, https://doi.org/10.1038/NATREVMATS.2016.103.
[157] B. Huang, B. Xu, Y. Li, W. Zhou, Y. You, S. Zhong, C.A. Wang, J.B. Goodenough, Li-Ion conduction and stability of perovskite Li3/8Sr7/16Hf1/4Ta3/4O3, ACS Appl. Mater. Interfaces 8 (23) (2016) 14552–14557, https://doi.org/10.1021/ACSAMI.6B03070/ASSET/IMAGES/LARGE/AM-2016-03070Q_0006.JPEG.
[158] K. Yu, Y. Tian, R. Gu, L. Jin, R. Ma, H. Sun, Y. Xu, Z. Xu, X. Wei, Ionic conduction, colossal permittivity and dielectric relaxation behavior of solid electrolyte Li3xLa2/3-xTiO3 ceramics, J. Eur. Ceram. Soc. 38 (13) (2018) 4483–4487, https://doi.org/10.1016/J.JEURCERAMSOC.2018.05.023.
[159] Lin C. an, M. Ihrig, Kung K. chen, Chen H. ching, W.S. Scheld, R. Ye, M. Finsterbusch, O. Guillon, Lin S. kang, Low-Temperature sintering of Li0.33La0.55TiO3 electrolyte for All-Solid-State li batteries, J. Eur. Ceram. Soc.

43 (16) (2023) 7543–7552, https://doi.org/10.1016/J.JEURCERAMSOC.2023.08.018.
[160] J.F. Wu, X. Guo, Size effect in nanocrystalline Lithium-Ion conducting perovskite: Li0.30La0.57TiO3, Solid State Ion. 310 (2017) 38–43, https://doi.org/10.1016/J.SSI.2017.08.003.
[161] J. Luo, S. Zhong, Z. Huang, B. Huang, C.A. Wang, High Li+-Conductive perovskite Li3/8Sr7/16Ta3/4Zr1/4O3 electrolyte prepared by Hot-Pressing for All-Solid-State Li-Ion batteries, Solid State Ion. 338 (2019) 1–4, https://doi.org/10.1016/J.SSI.2019.04.010.
[162] L. Li, J. Andrews, R. Mitchell, D. Button, D.C. Sinclair, I.M. Reaney, Aqueous cold sintering of Li-Based compounds, ACS Appl. Mater. Interfaces 15 (16) (2023) 20228–20239, https://doi.org/10.1021/ACSAMI.3C00392/SUPPL_FILE/AM3C00392_SI_001.PDF.
[163] S. Kim, H. Lee, J. Park, M. Ku, M. Kim, Y.-B. Kim, Lithium-Preserved sintering method for Perovskite-Based solid electrolyte thin films via flash light sintering for All-Solid-State Lithium-Ion batteries, J. Mater. Chem. A 11 (40) (2023) 21586–21594, https://doi.org/10.1039/D3TA03685E.
[164] H.X. Geng, A. Mei, C. Dong, Y.H. Lin, C.W. Nan, Investigation of structure and electrical properties of Li0.5La0.5TiO3 ceramics via microwave sintering, J. Alloy. Compd. 481 (1–2) (2009) 555–558, https://doi.org/10.1016/J.JALLCOM.2009.03.038.
[165] T. Polczyk, W. Zaj\c ac, M. Zi\c abka, K. Świerczek, Mitigation of grain boundary resistance in La2/3-xLi3xTiO3 perovskite as an electrolyte for Solid-State Li-Ion batteries, J. Mater. Sci. 56 (3) (2021) 2435–2450, https://doi.org/10.1007/S10853-020-05342-7/FIGURES/9.
[166] Z. Yao, K. Zhu, J. Zhang, J. Li, X. Li, J. Wang, K. Yan, J. Liu, LiF-Assisted synthesis of Perovskite-Type Li0.35La0.55TiO3 solid electrolyte for rechargeable Lithium-Metal batteries, J. Electron. Mater. 51 (2) (2022) 736–744, https://doi.org/10.1007/S11664-021-09331-7/FIGURES/5.
[167] X. Xu, S. Li, X. Wang, Y. Ma, X. Wang, K. Gao, Fabrication and characterization of Ca2Fe2O5 nanofibers photocatalyst by Sol-Gel assisted electrospinning at Low-Temperature, Mater. Lett. 143 (2015) 75–79, https://doi.org/10.1016/j.matlet.2014.12.065.
[168] T. Liu, S. Zhao, Q. Xiong, J. Yu, J. Wang, G. Huang, M. Ni, X. Zhang, Reversible discharge products in Li–Air batteries, Adv. Mater. 35 (20) (2023) 2208925, https://doi.org/10.1002/ADMA.202208925.
[169] Q. Ji, L. Bi, J. Zhang, H. Cao, X.S. Zhao, The role of oxygen vacancies of ABO3 perovskite oxides in the oxygen reduction reaction, Energy Environ. Sci. 13 (5) (2020) 1408–1428, https://doi.org/10.1039/D0EE00092B.
[170] Z. Zhu, S. Wan, Q. Lu, Q. Zhong, Y. Zhao, Y. Bu, A highly efficient perovskite oxides composite as a functional catalyst for tetracycline degradation, Sep. Purif. Technol. 281 (2022) 119893, https://doi.org/10.1016/j.seppur.2021.119893.
[171] P. Anand, D. Prabu Jaihindh, W.-K. Chang, Y.-P. Fu, Tailoring the Ca-Doped bismuth ferrite for electrochemical oxygen evolution reaction and photocatalytic activity, Appl. Surf. Sci. 540 (2021) 148387, https://doi.org/10.1016/j.apsusc.2020.148387.
[172] X. Xu, W. Wang, W. Zhou, Z. Shao, Recent advances in novel nanostructuring methods of perovskite electrocatalysts for Energy-Related applications, Small Methods 2 (7) (2018) 1800071, https://doi.org/10.1002/SMTD.201800071.
[173] X. Li, T. Zhu, C. Wen, Y. Yang, S. Ma, X. Huang, H. Li, G. Sun, Mixed spinel and perovskite phased LaSrNiO nanoparticles as cathode catalyst for Non-Aqueous Lithium-Oxygen batteries, Electrochim. Acta 317 (2019) 367–374, https://doi.org/10.1016/J.ELECTACTA.2019.05.054.
[174] M. Fang, X. Yao, W. Li, Y. Li, M. Shui, J. Shu, The investigation of lithium doping perovskite oxide LiMnO3 as possible LIB anode material, Ceram. Int. 44 (7) (2018) 8223–8231, https://doi.org/10.1016/J.CERAMINT.2018.02.002.
[175] D. Chen, L. Pan, P. Pei, X. Song, P. Ren, L. Zhang, Cobalt-Based oxygen electrocatalysts for Zinc-Air batteries: recent progress, challenges, and perspectives, Nano Res. 15 (6) (2022) 5038–5063, https://doi.org/10.1007/S12274-022-4154-4.
[176] P. Sennu, V. Aravindan, K.S. Nahm, Y.S. Lee, Exceptional catalytic activity of hollow structured La0.6Sr0.4CoO3−δ perovskite spheres in aqueous media and aprotic Li–O2 batteries, J. Mater. Chem. A 5 (34) (2017) 18029–18037, https://doi.org/10.1039/C7TA04189F.
[177] H. Dong, Y. Kiros, D. Noréus, An Air–Metal hydride battery using MmNi3.6Mn0.4Al0.3Co0.7 in the anode and a perovskite in the cathode, Int. J. Hydrog. Energy 35 (9) (2010) 4336–4341, https://doi.org/10.1016/J.IJHYDENE.2010.02.007.
[178] M. Christy, H. Rajan, H. Yang, Y.B. Kim, Optimizing the surface characteristics of La0.6Sr0.4CoO3−δ perovskite oxide by rapid flash sintering technology for easy fabrication and fast reaction kinetics in alkaline medium, Energy Fuels 34 (12) (2020) 16838–16846, https://doi.org/10.1021/ACS.ENERGYFUELS.0C03147/ASSET/IMAGES/LARGE/EF0C03147_0006.JPEG.
[179] E. Fabbri, D. Pergolesi, E. Traversa, Materials challenges toward Proton-Conducting oxide fuel cells: a critical review, Chem. Soc. Rev. 39 (11) (2010) 4355–4369, https://doi.org/10.1039/b902343g.
[180] E.D. Wachsman, K.T. Lee, Lowering the temperature of solid oxide fuel cells, Science 334 (6058) (2011) 935–939, https://doi.org/10.1126/SCIENCE.1204090/SUPPL_FILE/WACHSMAN_SOM.PDF.
[181] G. Kaur, Y. Cheng, M. Kaur, Brownmillerite and aurivillius electrolytes for intermediate temperature solid oxide fuel cell, Intermed. Temp. Solid Oxide Fuel Cells. Electrolytes Electrodes Interconnects (2020) 57–79, https://doi.org/10.1016/B978-0-12-817445-6.00002-8.
[182] M. Rafique, N. Safdar, M. Irshad, M. Usman, M. Akhtar, M.W. Saleem, M. M. Abbas, A. Ashour, M.E. Soudagar, Influence of low sintering temperature on BaCe0.2Zr0.6Y0.2O3−δ IT-SOFC perovskite electrolyte synthesized by Co-Precipitation method, Materials 15 (10) (2022) 3585, https://doi.org/10.3390/MA15103585.
[183] M.K. Hossain, M.C. Biswas, R.K. Chanda, M.H.K. Rubel, M.I. Khan, K. Hashizume, A review on experimental and theoretical studies of perovskite barium zirconate proton conductors, Emergent Mater. 4 (4) (2021) 999–1027, https://doi.org/10.1007/S42247-021-00230-5.
[184] M. Ab Rahman, M.H.D. Othman, H. Fansuri, Z. Harun, S.M. Jamil, A.F. Omar, M. A Rahman, J. Jaafar, A.F. Ismail, Effect of sintering temperature on Perovskite-Based hollow fiber as a substrate for Cathode-Supported Micro-Tubular solid oxide fuel cell, J. Aust. Ceram. Soc. 57 (4) (2021) 1199–1208, https://doi.org/10.1007/S41779-021-00620-2/METRICS.
[185] R.S. Pessoa, M.A. Fraga, W. Chiappim, H.S. Maciel, Exploring the properties and fuel cell applications of ultrathin atomic layer deposited metal oxide films, Emerg. Mater. Energy Convers. Storage (2018) 83–114, https://doi.org/10.1016/B978-0-12-813794-9.00003-X.
[186] X. Nie, Y. Chen, N. Mushtaq, S. Rauf, B. Wang, W. Dong, X. Wang, H. Wang, B. Zhu, The sintering temperature effect on electrochemical properties of Ce0.8Sm0.05Ca0.15O2-δ (SCDC)-La0.6Sr0.4Co0.2Fe0.8O3-δ (LSCF) heterostructure pellet, Nanoscale Res. Lett. 14 (1) (2019) 1–11, https://doi.org/10.1186/S11671-019-2979-X/FIGURES/6.
[187] S. Wang, J. Xu, M. Wu, Z. Song, L. Wang, L. Zhang, J. Yang, W. Long, L. Zhang, Cobalt–Free perovskite cathode BaFe0.9Nb0.1O3–δ for Intermediate–Temperature solid oxide fuel cell, J. Alloy. Compd. 872 (2021) 159701, https://doi.org/10.1016/J.JALLCOM.2021.159701.
[188] K.S. Baek, S.W. Baek, H. Kang, W. Choi, J.Y. Park, S. Saxin, S.K. Lee, J.H. Kim, Electrical conductivity characteristics of sr substituted layered perovskite cathode (SmBa0.5Sr0.5Co2O5+d) for intermediate Temperature-Operating solid oxide fuel cell, Ceram. Int. 48 (11) (2022) 15770–15779, https://doi.org/10.1016/j.ceramint.2022.02.114.
[189] W. Zając, D. Rusinek, K. Zheng, J. Molenda, Applicability of Gd-Doped BaZrO 3, SrZrO 3, BaCeO 3 and SrCeO 3 proton conducting perovskites as electrolytes for solid oxide fuel cells, Cent. Eur. J. Chem. 11 (4) (2013) 471–484, https://doi.org/10.2478/S11532-012-0144-9/MACHINEREADABLECITATION/RIS.
[190] K. Singh, A.K. Baral, V. Thangadurai, Grain boundary space charge effect and proton dynamics in chemically stable Perovskite-Type Ba0.5Sr0.5Ce0.6Zr0.2Gd0.1Y0.1O3-δ (BSCZGY): a case study on effect of sintering temperature, J. Am. Ceram. Soc. 99 (3) (2016) 866–875, https://doi.org/10.1111/jace.14008.
[191] S. Rauf, B. Zhu, M.A.K.Y. Shah, C. Xia, Z. Tayyab, N. Ali, C. Yang, N. Mushtaq, M. I. Asghar, F. Akram, P.D. Lund, Tailoring triple charge conduction in BaCo0.2Fe0.1Ce0.2Tm0.1Zr0.3Y0.1O3−δ semiconductor electrolyte for boosting solid oxide fuel cell performance, Renew. Energy 172 (2021) 336–349, https://doi.org/10.1016/J.RENENE.2021.03.031.
[192] Y. Gu, G. Luo, Z. Chen, Y. Huo, F.Z. Wu, Enhanced chemical stability and electrochemical performance of BaCe0.8Y0.1Ni0.04Sm0.06O3-δ perovskite electrolytes as proton conductors, Ceram. Int. 48 (8) (2022) 10650–10658, https://doi.org/10.1016/J.CERAMINT.2021.12.279.
[193] F. Zhao, S. Wang, L. Dixon, F. Chen, Novel BaCe0.7In0.2Yb0.1O3−δ proton conductor as electrolyte for intermediate temperature solid oxide fuel cells, J. Power Sources 196 (18) (2011) 7500–7504, https://doi.org/10.1016/J.JPOWSOUR.2011.04.036.
[194] Z. Zhang, L. Chen, Q. Li, T. Song, J. Su, B. Cai, H. He, High performance in, ta and Y-Doped BaCeO3 electrolyte membrane for Proton-Conducting solid oxide fuel cells, Solid State Ion. 323 (2018) 25–31, https://doi.org/10.1016/J.SSI.2018.04.021.
[195] T. Amiri, K. Singh, N.K. Sandhu, A.R. Hanifi, T.H. Etsell, J.-L. Luo, V. Thangadurai, P. Sarkar, High performance tubular solid oxide fuel cell based on ba 0.5 sr 0.5 ce 0.6 zr 0.2 gd 0.1 y 0.1 o 3-δ proton conducting electrolyte, J. Electrochem. Soc. 165 (10) (2018) F764–F769, https://doi.org/10.1149/2.0331810jes.
[196] J. Dang, Z. Zhu, J. Qian, W. Liu, A stable BaCe0.7Ta0.1In0.2O3−δ electrolyte membrane for Proton-Conducting solid oxide fuel cells, Ceram. Int. 39 (4) (2013) 4287–4292, https://doi.org/10.1016/J.CERAMINT.2012.11.008.
[197] G. Taillades, P. Pers, V. Mao, M. Taillades, High performance Anode-Supported proton ceramic fuel cell elaborated by wet powder spraying, Int. J. Hydrog. Energy 41 (28) (2016) 12330–12336, https://doi.org/10.1016/j.ijhydene.2016.05.094.
[198] F. Maglia, U. Anselmi-Tamburini, G. Chiodelli, H.E. Çamurlu, M. Dapiaggi, Z. A. Munir, Electrical, structural, and microstructural characterization of nanometric La0.9Sr0.1Ga0.8Mg0.2O3 − δ (LSGM) prepared by High-Pressure spark plasma sintering, Solid State Ion. 180 (1) (2009) 36–40, https://doi.org/10.1016/J.SSI.2008.10.005.
[199] A. Raghvendra, R. Kumar Singh, A.S.K. Sinha, P. Singh, Investigations on structural and electrical properties of calcium substituted LSGM electrolyte materials for IT-SOFC, Ceram. Int. 40 (7) (2014) 10711–10718, https://doi.org/10.1016/J.CERAMINT.2014.03.058.
[200] M.A.K.Y. Shah, S. Rauf, N. Mushtaq, Z. Tayyab, N. Ali, M. Yousaf, Y. Xing, M. Akbar, P.D. Lund, C.P. Yang, B. Zhu, M.I. Asghar, Semiconductor Fe-Doped SrTiO3-δ perovskite electrolyte for Low-Temperature solid oxide fuel cell (LT-SOFC) operating below 520 °C, Int. J. Hydrog. Energy 45 (28) (2020) 14470–14479, https://doi.org/10.1016/j.ijhydene.2020.03.147.
[201] M.A.K.Y. Shah, S. Rauf, B. Zhu, N. Mushtaq, M. Yousaf, P.D. Lund, C. Xia, M. I. Asghar, Semiconductor Nb-Doped SrTiO3-δPerovskite electrolyte for a ceramic fuel cell, ACS Appl. Energy Mater. 4 (1) (2021) 365–375, https://doi.org/10.1021/acsaem.0c02289.

[202] Z. Zhong, X. Xu, Z. Zhang, J. Li, X. Guo, S. Wu, H. Sun, Microwave sintering of High-Performance BaZr0.1Ce0.7Y0.1Yb0.1O3-δ (BZCYYb) electrolytes for Intermediate-Temperature solid oxide fuel cells, Int. J. Hydrog. Energy 47 (60) (2022) 25367–25377, https://doi.org/10.1016/J.IJHYDENE.2022.05.292.
[203] R. Li, F. Jin, Y. Zhang, B. Niu, J. Liu, T. He, Performance and optimization of Perovskite-Type La1·4Ca0·6CoMnO5+δ cathode for Intermediate-Temperature solid oxide fuel cells, Int. J. Hydrog. Energy 44 (16) (2019) 8467–8478, https://doi.org/10.1016/J.IJHYDENE.2019.01.296.
[204] S. Wang, J. Zan, W. Qiu, D. Zheng, F. Li, W. Chen, Q. Pei, L. Jiang, Evaluation of perovskite oxides LnBaCo2O5+δ (Ln = La, Pr, Nd and Sm) as cathode materials for IT-SOFC, J. Electroanal. Chem. 886 (2021) 115144, https://doi.org/10.1016/J.JELECHEM.2021.115144.
[205] N. Hou, J. Gan, Q. Yan, Y. Zhao, Y. Li, Improved electrochemical oxidation kinetics of La0.5Ba0.5FeO3-δ anode for solid oxide fuel cells with fluorine doping, J. Power Sources 521 (2022) 230932, https://doi.org/10.1016/J.JPOWSOUR.2021.230932.
[206] F. Zurlo, A. Iannaci, V.M. Sglavo, E. Di Bartolomeo, Copper-Based electrodes for IT-SOFC, J. Eur. Ceram. Soc. 39 (1) (2019) 17–20, https://doi.org/10.1016/J.JEURCERAMSOC.2018.02.029.
[207] W. Yang, T. Hong, S. Li, Z. Ma, C. Sun, C. Xia, L. Chen, Perovskite Sr1-xCexCoO3-δ (0.05 ≤ x ≤ 0.15) as superior cathodes for intermediate temperature solid oxide fuel cells, ACS Appl. Mater. Interfaces 5 (3) (2013) 1143–1148, https://doi.org/10.1021/AM3029238/ASSET/IMAGES/LARGE/AM-2012-029238_0010.JPEG.
[208] S. Park, S. Choi, J. Shin, G. Kim, Tradeoff optimization of electrochemical performance and thermal expansion for Co-Based cathode material for Intermediate-Temperature solid oxide fuel cells, Electrochim. Acta 125 (2014) 683–690, https://doi.org/10.1016/J.ELECTACTA.2014.01.112.
[209] F. Jin, Y. Shen, R. Wang, T. He, Double-Perovskite PrBaCo2/3Fe2/3Cu2/3O5+δ as cathode material for Intermediate-Temperature Solid-Oxide fuel cells, J. Power Sources 234 (2013) 244–251, https://doi.org/10.1016/J.JPOWSOUR.2013.01.172.
[210] S. en Hou, J.A. Alonso, J.B. Goodenough, Co-Free, iron perovskites as cathode materials for Intermediate-Temperature solid oxide fuel cells, J. Power Sources 195 (1) (2010) 280–284, https://doi.org/10.1016/J.JPOWSOUR.2009.07.017.
[211] H. Liu, K. Zhu, Y. Liu, W. Li, L. Cai, X. Zhu, M. Cheng, W. Yang, Structure and electrochemical properties of Cobalt-Free perovskite cathode materials for Intermediate-Temperature solid oxide fuel cells, Electrochim. Acta 279 (2018) 224–230, https://doi.org/10.1016/J.ELECTACTA.2018.05.086.
[212] H. Cai, L. Zhang, J. Xu, J. Huang, X.L. Wei, L. Wang, Z. Song, W. Long, Cobalt–Free La0.5Sr0.5Fe0.9Mo0.1O3–δ electrode for symmetrical SOFC running on H2 and CO fuels, Electrochim. Acta 320 (2019) 134642, https://doi.org/10.1016/J.ELECTACTA.2019.134642.
[213] L. Miao, J. Hou, Z. Gong, Z. Jin, W. Liu, A High-Performance Cobalt-Free Ruddlesden-Popper phase cathode La1·2Sr0·8Ni0·6Fe0·4O4+δ for low temperature Proton-Conducting solid oxide fuel cells, Int. J. Hydrog. Energy 44 (14) (2019) 7531–7537, https://doi.org/10.1016/J.IJHYDENE.2019.01.255.
[214] S. Liu, W. Menglin, L. Lu, J. Ni, C. Ni, J.T.S. Irvine, La0.5Ba0.5CuxFe1−xO3−δ as cathode for High-Performance Proton-Conducting solid oxide fuel cell, Sep. Purif. Technol. 297 (2022) 121485, https://doi.org/10.1016/J.SEPPUR.2022.121485.
[215] F. Dong, Y. Chen, R. Ran, D. Chen, M.O. Tadé, S. Liu, Z. Shao, BaNb0.05Fe0.95O3−δ as a new oxygen reduction electrocatalyst for intermediate temperature solid oxide fuel cells, J. Mater. Chem. A 1 (34) (2013) 9781–9791, https://doi.org/10.1039/C3TA11447C.
[216] M. Bilal Hanif, M. Motola, S. Qayyum, S. Rauf, A. Khalid, C.J. Li, C.X. Li, Recent advancements, doping strategies and the future perspective of Perovskite-Based solid oxide fuel cells for energy conversion, Chem. Eng. J. 428 (2022) 132603, https://doi.org/10.1016/J.CEJ.2021.132603.
[217] V. Cascos, L. Troncoso, J.A. Alonso, M.T. Fernández-Díaz, Design of new Ga-Doped SrMoO3 perovskites performing as anode materials in SOFC, Renew. Energy 111 (2017) 476–483, https://doi.org/10.1016/J.RENENE.2017.04.023.
[218] Abdalla, A.M.; Hossain, S.; Mohd, P.; Petra, I.; Savaniu, C.D.; Irvine, J.T.S.; Azad, A.K. Novel Layered Perovskite SmBaMn 2 O 5+d for SOFCs Anode Material. 2017. ⟨https://doi.org/10.1016/j.matlet.2017.06.029⟩.
[219] T. Xia, A. Brüll, A. Grimaud, S. Fourcade, F. Mauvy, H. Zhao, J.C. Grenier, J. M. Bassat, Optimization of the electrochemical performance of a Ni/Ce0.9Gd0.1O2−δ-Impregnated La0.57Sr0.15TiO3 anode in hydrogen, Solid State Sci. 35 (2014) 1–9, https://doi.org/10.1016/J.SOLIDSTATESCIENCES.2014.06.008.
[220] F. Liu, L. Zhang, G. Huang, B. Niu, X. Li, L. Wang, J. Zhao, Y. Jin, High performance Ferrite–Based anode La0.5Sr0.5Fe0.9Mo0.1O3–δ for Intermediate–Temperature solid oxide fuel cell, Electrochim. Acta 255 (2017) 118–126, https://doi.org/10.1016/J.ELECTACTA.2017.09.157.
[221] Y. Zheng, J. Wang, B. Yu, W. Zhang, J. Chen, J. Qiao, J. Zhang, A review of high temperature Co-Electrolysis of H2O and CO2 to produce sustainable fuels using solid oxide electrolysis cells (SOECs): advanced materials and technology, Chem. Soc. Rev. 46 (2017) 1427–1463, https://doi.org/10.1039/c6cs00403b.
[222] L. Bi, S. Boulfrad, E. Traversa, Steam electrolysis by solid oxide electrolysis cells (SOECs) with Proton-Conducting oxides, Chem. Soc. Rev. 43 (2014) 8255–8270, https://doi.org/10.1039/c4cs00194j.
[223] S. Rajendran, N.K. Thangavel, S. Alkatie, Y. Ding, L.M.R. Arava, Y, gd, and pr Tri-Doped Perovskite-Type proton conducting electrolytes with improved sinterability and chemical stability, J. Alloy. Compd. 870 (2021) 159431, https://doi.org/10.1016/J.JALLCOM.2021.159431.
[224] A. Hauch, R. Küngas, P. Blennow, A.B. Hansen, J.B. Hansen, B.V. Mathiesen, M. B. Mogensen, Recent advances in solid oxide cell technology for electrolysis, Science 370 (6513) (2020), https://doi.org/10.1126/SCIENCE.ABA6118/ASSET/1FC1B2A5-65CC-4804-B1E0-300396997D05/ASSETS/GRAPHIC/370_ABA6118_F5.JPEG.
[225] X. Zhang, B. Liu, Y. Yang, J. Li, J. Li, Y. Zhao, L. Jia, Y. Sun, Advances in component and operation optimization of solid oxide electrolysis cell, Chin. Chem. Lett. 34 (5) (2023) 108035, https://doi.org/10.1016/J.CCLET.2022.108035.
[226] S. Kim, S.W. Lee, S. Lee, J.H. Kim, T.H. Shin, Revolutionizing hydrogen production with LSGM-Based solid oxide electrolysis cells: an innovative approach by sonic spray, Electrochim. Acta 463 (2023) 142751, https://doi.org/10.1016/J.ELECTACTA.2023.142751.
[227] S.Y. Gómez, D. Hotza, Current developments in reversible solid oxide fuel cells, Renew. Sustain. Energy Rev. 61 (2016) 155–174, https://doi.org/10.1016/j.rser.2016.03.005.
[228] Z. Tan, T. Ishihara, Infiltrated Nano-CeO2 and inserted Ni-Fe active layer in a tubular cathode substrate for high temperature CO2 electrolysis on solid oxide cells using La0.9Sr0.1Ga0.8Mg0.2O3−δ thin film electrolyte, Electrochim. Acta 424 (2022) 140506, https://doi.org/10.1016/J.ELECTACTA.2022.140506.
[229] Q. Liu, C. Yang, X. Dong, F. Chen, Perovskite Sr2Fe1.5Mo0.5O6−δ as electrode materials for symmetrical solid oxide electrolysis cells, Int. J. Hydrog. Energy 35 (19) (2010) 10039–10044, https://doi.org/10.1016/J.IJHYDENE.2010.08.016.
[230] Y. Wang, T. Liu, M. Li, C. Xia, B. Zhou, F. Chen, Exsolved Fe-Ni Nano-Particles from Sr2Fe1.3Ni0.2Mo0.5O6 perovskite oxide as a cathode for solid oxide steam electrolysis cells, J. Mater. Chem. A 4 (37) (2016) 14163–14169, https://doi.org/10.1039/c6ta06078a.
[231] H. Bai, Y. Zhang, J. Chu, Q. Zhou, H. Lan, J. Zhou, Oxygen electrode PrBa0.5Sr0.5Co1.5Fe0.5O5+δ-BaZr0.1Ce0.7Y0.1Yb0.1O3−δ with different composite proportions for Proton-Conducting solid oxide electrolysis cells, ACS Appl. Mater. Interfaces 15 (32) (2023) 38581–38591, https://doi.org/10.1021/acsami.3c07638.
[232] W. Li, B. Guan, L. Ma, H. Tian, X. Liu, Synergistic coupling of proton conductors BaZr0.1Ce0.7Y0.1Yb0.1O3-δ and La2Ce2O7 to create chemical stable, interface active electrolyte for steam electrolysis cells, ACS Appl. Mater. Interfaces 11 (20) (2019) 18323–18330, https://doi.org/10.1021/ACSAMI.9B00303/ASSET/IMAGES/LARGE/AM-2019-00303Q_0002.JPEG.
[233] S. Choi, T.C. Davenport, S.M. Haile, Protonic ceramic electrochemical cells for hydrogen production and electricity generation: exceptional reversibility, stability, and demonstrated faradaic efficiency, Energy Environ. Sci. 12 (1) (2019) 206–215, https://doi.org/10.1039/C8EE02865F.
[234] D. Huan, W. Wang, Y. Xie, N. Shi, Y. Wan, C. Xia, R. Peng, Y. Lu, Investigation of real polarization resistance for electrode performance in Proton-Conducting electrolysis cells, J. Mater. Chem. A 6 (38) (2018) 18508–18517, https://doi.org/10.1039/c8ta06862c.
[235] L. Lei, J. Zhang, Z. Yuan, J. Liu, M. Ni, F. Chen, Progress report on proton conducting solid oxide electrolysis cells, Adv. Funct. Mater. 29 (37) (2019) 1903805, https://doi.org/10.1002/ADFM.201903805.
[236] Y. Huang, J. Yu, N. Tian, Y. Qu, W. Tan, Y. Luo, C. Wang, R. Zheng, J. Zheng, Performance study of proton conducting electrolytes based on BaZr1−xYxO3-δ for solid oxide electrolysis cell, Int. J. Electrochem. Sci. 18 (3) (2023) 100033, https://doi.org/10.1016/J.IJOES.2023.100033.
[237] Z. Leng, Z. Huang, X. Zhou, B. Zhang, H. Bai, J. Zhou, S. Wang, The effect of sintering aids on BaCe0·7Zr0·1Y0.1Yb0.1O3-δ as the electrolyte of Proton-Conducting solid oxide electrolysis cells, Int. J. Hydrog. Energy 47 (79) (2022) 33861–33871, https://doi.org/10.1016/J.IJHYDENE.2022.07.237.
[238] Y. Gou, Y. Zhao, J. Zhang, W. Sun, J. Qiao, K. Sun, Z. Wang, One-Step synthesis and densification uniform BaZr0.1Ce0.7Y0.1Yb0.1O3-δ by Step-Wise current reactive flash sintering, Ceram. Int. 48 (23) (2022) 35108–35114, https://doi.org/10.1016/J.CERAMINT.2022.08.106.
[239] M. Chen, D. Chen, K. Wang, Q. Xu, Densification and electrical conducting behavior of BaZr0.9Y0.1O3-δ proton conducting ceramics with NiO additive, J. Alloy. Compd. 781 (2019) 857–865, https://doi.org/10.1016/J.JALLCOM.2018.12.090.
[240] R.M. Matsuda, K. Nakamura, M. Mori, J. Dailly, Sintering mechanism and electrical conductivity of ZnO added BaCe0.8Zr0.1Y0.1O3-δ proton conducting perovskites, Solid State Ion. 403 (2023) 116407, https://doi.org/10.1016/J.SSI.2023.116407.
[241] R. Wang, G.Y. Lau, D. Ding, T. Zhu, M.C. Tucker, Approaches for Co-Sintering Metal-Supported Proton-Conducting solid oxide cells with Ba(Zr,Ce,Y,Yb)O3-δ electrolyte, Int. J. Hydrog. Energy 44 (26) (2019) 13768–13776, https://doi.org/10.1016/J.IJHYDENE.2019.03.181.
[242] D.J. Deka, S. Gunduz, T. Fitzgerald, J.T. Miller, A.C. Co, U.S. Ozkan, Production of syngas with controllable H2/CO ratio by high temperature Co-Electrolysis of CO2 and H2O over ni and Co- doped lanthanum strontium ferrite perovskite cathodes, Appl. Catal. B Environ. 248 (2019) 487–503, https://doi.org/10.1016/J.APCATB.2019.02.045.
[243] B. Qian, S. Wang, Y. Zheng, Q. Ni, H. Chen, L. Ge, J. Yang, Ca-Fe Co-Doped La0.75Sr0.25Cr0.5Mn0.5O3 cathodes with high electrocatalytic activity for direct CO2 electrolysis in solid oxide electrolysis cells, J. CO2 Util. 67 (2023) 102305, https://doi.org/10.1016/J.JCOU.2022.102305.
[244] K. Leonard, J. Druce, V. Thoreton, J.A. Kilner, H. Matsumoto, Exploring mixed Proton/Electron conducting air electrode materials in protonic electrolysis cell, Solid State Ion. 319 (2018) 218–222, https://doi.org/10.1016/J.SSI.2018.02.016.
[245] H. Jiang, Z. Lu, B. Qian, S. Wang, B. Yin, Y. Zheng, L. Ge, H. Chen, C. Zhang, Bi-Doped La1.5Sr0.5Ni0.5Mn0.5O4+δ as an efficient air electrode material for SOEC, Int. J. Hydrog. Energy 46 (73) (2021) 36037–36045, https://doi.org/10.1016/J.IJHYDENE.2021.08.144.

[246] H. Dai, E.H. Da'as, S.P. Shafi, H. Wang, L. Bi, Tailoring cathode composite boosts the performance of Proton-Conducting SOFCs fabricated by a One-Step Co-Firing method, J. Eur. Ceram. Soc. 38 (7) (2018) 2903–2908, https://doi.org/10.1016/J.JEURCERAMSOC.2018.02.022.

[247] E. Sánchez-Ahijón, R. Schmidt, X. Martínez de Irujo-Labalde, H.M. Ansari, M. T. Fernández-Díaz, E. Morán, B. Molero-Sánchez, J. Prado-Gonjal, Structural and dielectric properties of Ultra-Fast Microwave-Processed La0.3Ca0.7Fe0.7Cr0.3O3−δ ceramics, J. Solid State Chem. 314 (2022) 123426, https://doi.org/10.1016/J.JSSC.2022.123426.

[248] F. Liang, P. hung Tseng, Q. Sun, M. Li, W. Zhou, L.X. Liu, H. Wang, Z. Zhu, Microwave plasma rapid heating towards robust Cathode/Electrolyte interface for solid oxide fuel cells, J. Colloid Interface Sci. 607 (2022) 53–60, https://doi.org/10.1016/J.JCIS.2021.08.182.

[249] Q. Lin, L. Bian, C. Liu, T. Ting, Z. Liu, P. Wei, S. Han, Y. Xu, J. Peng, S. An, Improved La0.8Sr0.2MnO3-δ oxygen electrode activity by introducing high oxygen ion conductor oxide for solid oxide steam electrolysis, Int. J. Hydrog. Energy (2023), https://doi.org/10.1016/J.IJHYDENE.2023.08.316.

[250] P.K. Patro, T. Delahaye, E. Bouyer, Development of Pr0.58Sr0.4Fe0.8Co0.2O3 − δ–GDC composite cathode for solid oxide fuel cell (SOFC) application, Solid State Ion. 181 (29–30) (2010) 1378–1386, https://doi.org/10.1016/J.SSI.2010.07.004.

[251] H. Korkmaz, B. Timurkutluk, C. Timurkutluk, Effects of fabrication parameters on the performance of solid oxide electrolyzer cell, Int. J. Hydrog. Energy 41 (23) (2016) 9723–9730, https://doi.org/10.1016/J.IJHYDENE.2016.02.005.

[252] A.D.N. Kamkeng, M. Wang, Long-Term performance prediction of solid oxide electrolysis cell (SOEC) for CO2/H2O Co-Electrolysis considering structural degradation through modelling and simulation, Chem. Eng. J. 429 (2022) 132158, https://doi.org/10.1016/J.CEJ.2021.132158.

[253] K. Yang, Y. Wang, L. Jiang, Y. Jin, Z. Yang, Cobalt-Free perovskite Ba0.95La0.05FeO3-δ as efficient and durable oxygen electrode for solid oxide electrolysis cells, Int. J. Hydrog. Energy 48 (71) (2023) 27464–27472, https://doi.org/10.1016/J.IJHYDENE.2023.03.197.

[254] Y. Li, L. Yang, W. Li, Z. Hou, C. Shi, G. Zhang, J. Zhou, S. Wang, A promising strontium and Cobalt-Free air electrode Pr1-xCaxFeO3-δ for solid oxide electrolysis cell, Int. J. Hydrog. Energy 46 (59) (2021) 30230–30238, https://doi.org/10.1016/J.IJHYDENE.2021.06.185.

[255] Z. Teng, Z. Xiao, G. Yang, L. Guo, X. Yang, R. Ran, W. Wang, W. Zhou, Z. Shao, Efficient water splitting through solid oxide electrolysis cells with a new hydrogen electrode derived from A-Site Cation-Deficient La0.4Sr0.55Co0.2Fe0.6Nb0.2O3-δ perovskite, Mater. Today Energy 17 (2020), https://doi.org/10.1016/j.mtener.2020.100458.

[256] W. Qi, Y. Zhang, J. Cui, X. Shu, Y. Wang, Y. Wu, In-Situ constructing NiO nanoplatelets network on La0.75Sr0.25Mn0.5Cr0.5O3-δ electrode with enhanced steam electrolysis, Int. J. Hydrog. Energy 42 (9) (2017) 5657–5666, https://doi.org/10.1016/J.IJHYDENE.2016.12.097.

[257] G. Tsekouras, J.T.S. Irvine, The role of defect chemistry in strontium titanates utilised for high temperature steam electrolysis, J. Mater. Chem. (25) (2011) 9367–9376, https://doi.org/10.1039/c1jm11313e.

[258] N. Bimpiri, A. Konstantinidou, K.M. Papazisi, S. Balomenou, D. Tsiplakides, Electrochemical performance of iron doped lanthanum strontium chromites as fuel electrodes in high temperature solid oxide cells, Electrochim. Acta (2023) 143537, https://doi.org/10.1016/J.ELECTACTA.2023.143537.